COMPARISON OF COOLING LAKE MATHEMATICAL MODELS FOR MOUNT STORM LAKE

by

OLUTOYIN M. ADELAJA

and

E. ERIC ADAMS

DEPARTMENT OF CIVIL ENGINEERING

RALPH M. PARSONS LABORATORY

AQUATIC SCIENCE AND ENVIRONMENTAL ENGINEERING

SCHOOL OF ENGINEERING

MASSACHUSETTS INSTITUTE OF TECHNOLOGY

Cambridge, Massachusetts 02139

Report Number 328

Prepared under the support of

Virginia Power, Richmond, Virginia

March, 1990

R90-4

COMPARISON OF COOLING LAKE MATHEMATICAL MODELS FOR MOUNT STORM LAKE

by
OLUTOYIN M. ADELAJA
and
E. ERIC ADAMS

RALPH M. PARSONS LABORATORY
AQUATIC SCIENCE AND ENVIRONMENTAL ENGINEERING

Report Number 328

Prepared under the support of
Virginia Power, Richmond, Virginia

March, 1990

ABSTRACT

Mt. Storm Lake is an impoundment of the Stony River that provides cooling for the three-unit electric generating station which is owned by Virginia Power. The lake is relatively deep and narrow with a submerged intake and a surface discharge. Although the temperature structure in a cooling lake is usually three dimensional, it is often possible to use reduced dimension calculations to make sufficiently accurate predictions by dividing the lake into zones.

MITEMP is a time-dependent temperature model for cooling lakes consisting of a 1-D (longitudinal) surface layer overlying a 1-D (vertical) variable-area hypolimnion. This model was adapted to Mt. Storm Lake using available field data for calibration and verification. The initial model predictions, using data from Sept. 1986 - Aug. 1987 and made prior to our calibration, were quite good with average errors ranging from -0.1 to -1.1° C depending on location within the lake. Model calibration consisted of adjustments to the net solar radiation, as well as the entrance dilution coefficient and the surface layer longitudinal dispersion coefficient. The average errors after calibration were reduced to about 0-0.5° C with a standard deviation of 1-1.4° C. The residual time series of model errors after calibration was shown to be correlated to station generation, indicating that better model performance could be achieved by an improved representation of the heat rejection.

As part of a related study, a 0-D water and energy balance model was developed to assess water availability at Mount Storm Lake under several different scenarios. This model is very efficient, requiring less than five minutes of CPU time to do over 1000 years of simulation in comparison with about 3 minutes for a 1-year simulation with MITEMP. (Both are for a MicroVax II.) The temperature predictions of the 0-D model were evaluated to assess its accuracy as a screening model. Although the model is steady-state, it was shown theoretically and empirically to have similar thermal inertia to a transient model if 30-day (monthly averaged) data were used as input. Results show that the 0-D model predicts the lake temperature fairly accurately. The mean error varies between ±0.35° C for different averaging intervals between 10 and 40 days, and the standard deviation is 2.5° C using 30-day averaged data.

A preliminary comparison was also made between MITEMP and a 2-D (longitudinal and vertical transient model), NARES, to see what changes in thermal structure result from an improved description of the flow field. There was not time to complete this part of the study, but initial model predictions show reasonable agreement between observed and predicted longitudinal variation in hypolimnetic temperature. However, because the maximum observed longitudinal variation is only about 2.0° C, the added detail is not critical especially since the 2-D model is quite time consuming to run (about 14 hours of MicroVax II CPU time for an annual simulation). This is two-and-one-half orders of magnitude more expensive than MITEMP. However, there is the potential for this model to provide useful information if a new generating facility were to be added at a different location on the lake. However, it would require more calibration and validation effort.

Acknowledgments

This study was supported by Virginia Power, Richmond, Virginia. The cooperation of Jud White, Nat Wooding, and Bill Fraser is appreciated.

The report represents the Master's thesis of Ms. Olutoyin Adelaja, submitted to the Department of Civil Engineering at Massachusetts Institute of Technology. Thesis supervision was provided by Dr. E. Eric Adams, Principal Research Engineer and Lecturer in the Department of Civil Engineering. The authors are grateful to Mr. Read Schusky who typed the manuscript.

Table of Contents

List of Figures

List of Tables

1 WHY MATHEMATICAL MODELS

Mathematical models are an efficient and practical way to simulate, monitor, and evaluate the aquatic environment. They provide information on which to base important decisions and play a significant role in assessing the environmental effects of major projects.

For impoundments—whether natural or those used for cooling—the flow and temperature structure is generally three dimensional. Therefore 3-D models in which the full three-dimensional equations of motion are coupled with the corresponding three-dimensional heat transport and continuity equations are usually the most accurate. However, they are not necessarily the most efficient models. It is usually possible to adequately determine the parameters that are of engineering, biological, or legal interest by simpler 2-D, 1-D, or even 0-D models.

This study aims to develop a validated model of a cooling reservoir—Mt. Storm Lake, which provides cooling for the Mt. Storm Station in West Virginia—and to compare the model with alternative models having a range of complexity.

1.1 The Mount Storm Station

The station is a three-unit 1617-MWe coal-fired electric generating station that is owned by Virginia Power. Each of the three units is equipped with two circulating water pumps for the condenser water intake and discharge. The condenser cooling system takes water from near the bottom of the lake and discharges it at the surface. At 100% load, the average condenser temperature rise is 10.2° C and the circulating water flow rate is 49 m^3/s.

1.2 Characteristics of Mount Storm Lake

Mount Storm Lake is an impoundment of the Stony River in northern Grant County, West Virginia, (see Figure 1.1) created by Virginia Power to provide cooling for the Mount Storm Electric Generating Station. Virginia Power has an NPDES permit that limits the allowable temperature of discharge into the Stony River to 95° F (35° C). There are two spray modules located just prior to the spillway; the NPDES permit requires that they be operated whenever the surface temperature at the base of the spillway is 85° F (29.4° C) or greater.

The cooling lake has a surface area of about 1100 acres (445 ha) and a volume of 46,700 acre-feet ($57.6 \times 10^6 m^3$) when full. It has an average depth of about 40 feet (12 m) with a maximum depth of over 100 ft (30 m). The depth to the intakes is about 90 ft (27 m). Because the station intakes for the lake are located near the bottom and the discharge is near the surface, most of the volume of Mount Storm Lake is involved in the circulation resulting in good thermal inertia (reducing the magnitude of the temperature changes in response to fluctuating meteorology). The thermal loading rate at Mount Storm is 1.87 MWt/acre, which suggests that the lake is relatively heavily loaded when compared (see Table 1.1) to other cooling lakes.

Jirka et al. (1978) define a pond number, $\mathbb{P}$ (see Appendix A.1), which they use to classify cooling impoundments. They found that impoundments were vertically well mixed for $\mathbb{P} > 1$, partially mixed for $0.3 < \mathbb{P} < 1$, and vertically stratified for $\mathbb{P} < 0.3$. Since predictions for partially mixed shallow ponds in the range $0.3 < \mathbb{P} < 1$ are most difficult, the usual procedure is to extend the applicability of vertically stratified models up to $\mathbb{P} \leq 0.5$ and that of vertically fully mixed models down to $\mathbb{P} > 0.5$. For Mount Storm Lake $\mathbb{P} \simeq 0.3$ which suggests primarily vertical as opposed to

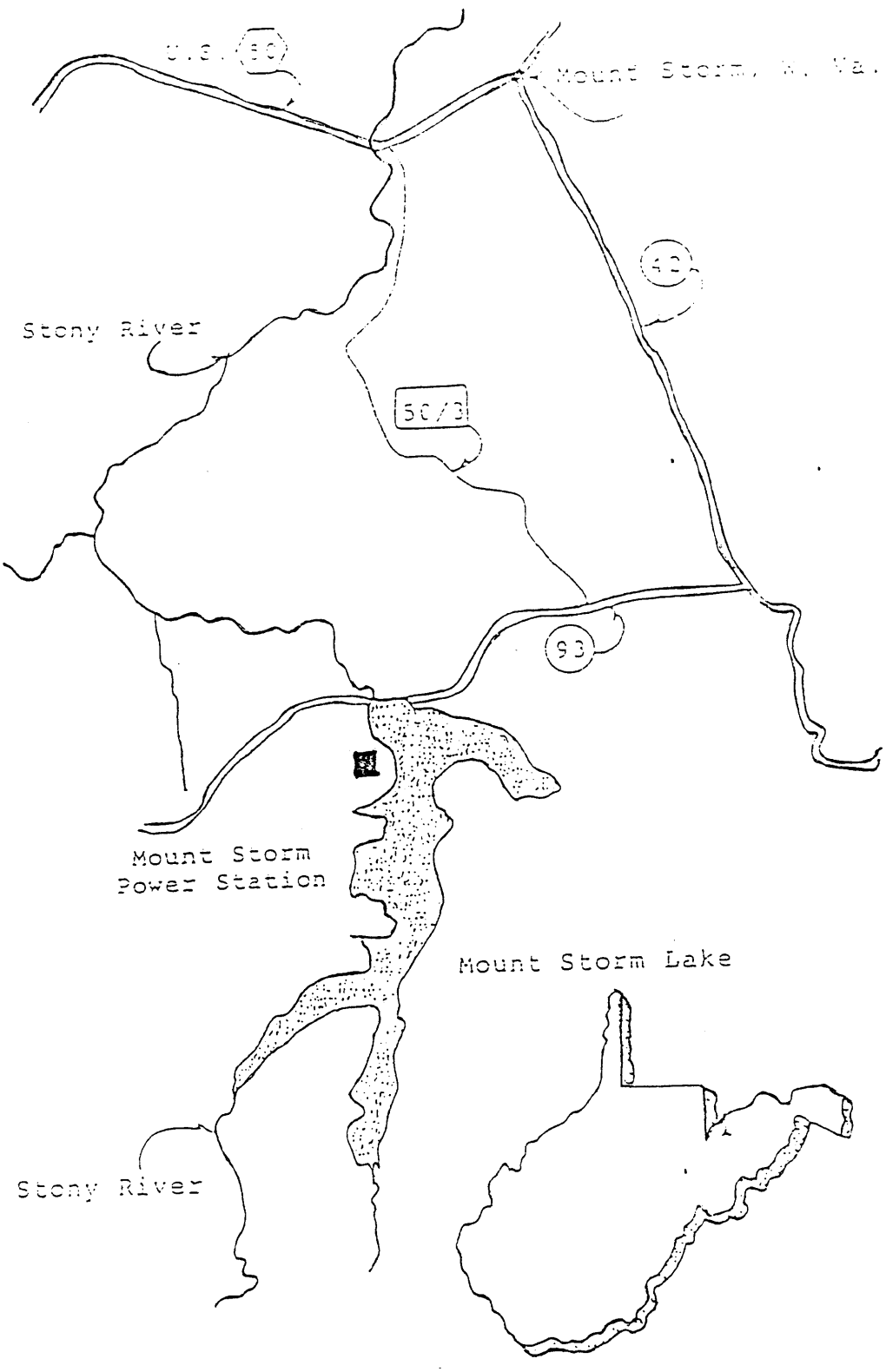

Figure 1-1 Vicinity map of Mount Storm Lake, West Virginia

Table 1.1

Comparison of Physical Characteristics for Typical Cooling Lakes and Ponds in the U.S.

Name of impoundment	Impoundment area (acres)	Station capacity (MWe)	Waste heat rejection (MWt)	Thermal loading (MWt/acre)
Cooling Lakes				
Lake Anna, Virginia	13,000	1,870 (Nuclear)	3,700	0.28
Clinton Lake, Illinois	4,895	1,982 (Nuclear)	3,750	0.77
Gibbons Creek, Reservoir, Texas	2,295	896 (Fossil)	1,170	0.51
Merom Lake, Indiana	1,550	980 (Fossil)	1,465	0.94
Mount Storm Lake, West Virginia	1,100	1,617 (Fossil)	2,058	1.87
Lake Robinson, North Carolina	2,250	135(Fossil) +730(Nuclear)	1,750	0.78
Lake Sanchris, Illinois	2,165	1,232 (Fossil)	1,930	0.89
Sutherland Reservoir, Nebraska	2,140	1,300 (Fossil)	2,040	0.95
Cooling Ponds				
Braidwood, Illinois	2,539	2,200 (Nuclear)	4,520	1.78
Collins, Illinois	2,009	2,520 (Fossil)	3,074	1.53
Dresden, Illinois	1,275	1,600 (Nuclear)	2,678	2.10
La Salle, Illinois	2,058	2,156 (Nuclear)	4,362	2.12
Powerton, Illinois	1,442	1,670 (Fossil)	2,437	1.69

horizontal stratification. This conclusion and field data generally support a 1-D (vertical variation only) structure except for some 2-D structure near the surface. Therefore the basic model structure uses the model MITEMP (Jirka et al., 1978) for deep artificially heated cooling ponds. This model is a quasi-1-D model that includes a surface layer with horizontal temperature variation overlying a deep, vertically stratified region. The model is discussed in greater detail in Chapter 2.

1.3 Objectives of the Study

Virginia Power is considering several options for increasing power generation at the Mount Storm Station. A reliable thermal model of the lake is therefore required to assess compliance for the existing as well as potential future options. Also a thermal model would be useful in assessing the biological impacts on the lake of station generation, and as a basis for any future water quality modeling.

The study consist of two parts. The first is to develop a good (calibrated and efficient) model of lake temperature for Virginia Power. This model is based on MITEMP and uses transient (daily averaged) meteorological plant operation and water temperature data collected during the last three years. The model is efficient, requiring only a few minutes of CPU time on a MicroVax computer for a year's simulation. Hence it can be readily used for utility planning purposes.

The second objective is to examine the relative advantages of using the 1-D model as compared with a more complex 2-D model and a simpler 0-D model.

A priori, it might be expected that the 2-D model could provide, at additional computer cost, useful information concerning the spatial temperature distribution in the pond which could help in evaluating the relative merits of alternative discharge and intake locations, appropriate locations to monitor compliance, etc. On the

other hand, the 0-D model might be useful as a screening tool to rapidly evaluate a range of scenarios using 10s or 100s of years of meteorological or hydrological input data.

2 DESCRIPTION OF 1-D MODEL MITEMP

This chapter describes the one-dimensional model MITEMP which was the focus of this study. Although some previous study of Mount Storm Lake had been performed (Gilbert/Commonwealth, 1985), that study assumed the lake was in a steady state. However, the nature of cooling and natural impoundments is transient. The processes that govern them are never in steady state but vary throughout the year depending both on meteorological conditions and, for cooling impoundments, on the heat rejected by the power plant. Thus a model that will simulate and predict these processes must be a transient one. As discussed in Chapter 1, the preliminary analysis of the lake suggests that the lake is predominantly vertically stratified resulting in a one-dimensional temperature structure below a shallow surface layer.

MITEMP is a package of one-dimensional time-varying sub-models developed at MIT. Each model includes the calculation of component heat transfer processes from the water surface to the atmosphere coupled with a description of the advective and diffusive mixing processes within the impoundment. The primary use of the models is in the design and simulation of cooling lakes or ponds for the dissipation of waste heat from steam-electric generating plants (Octavio et al., 1980). Mount Storm Lake may be described as a deep, vertically stratified cooling pond (using the method of pond classification described by Jirka et al. (1978)). Therefore, the deep stratified cooling pond submodel of MITEMP is described here. (See Jirka et al., 1978, for the description of other classes of models.)

While studying the behavior of relatively deep ponds, Ryan and Harleman (1973) found that surface density currents effectively spread heated water over the entire surface of the pond, even if there are distinct backwater "dead" areas. These

density currents result in a thin heated surface layer of thickness Δz_s, with horizontal temperature gradients due to cooling to the atmosphere. This layer overlies a horizontally uniform subsurface region, in which only vertical temperature variations occur due to the gradual advective flow to the submerged intakes (see Figure 2.1). Therefore essentially a 2-D structure is obtained by a combination of two one-dimensional models. This submodel takes into account inflows and outflows to the lake as well as the variation of horizontal area with depth.

2.1 Model Formulation

As described in the previous section, the deep stratified cooling pond submodel (of MITEMP) consists of two parts: the horizontally stratified surface layer and the vertically stratified subsurface layer.

2.1.1 Surface Layer

The surface layer is actually made up of two regions (see Jirka et al., 1977, 1978), the entrance mixing region and the surface layer region. The entrance mixing region is relatively small in comparison to the rest of the surface layer. It is used to represent the reduction in temperature that takes place in the vicinity of the discharge due to turbulent entrainment of the surrounding water into the discharge plume. This dilution is denoted by a dilution factor D_v. The mixed temperature obtained due to this dilution, T_m, is used as a boundary value for the surface layer region. Outside the mixing region, the surface layer region is also assumed to have a strong thermocline between the surface and subsurface layers. This prevents vertical diffusion and entrainment across the interface. The governing equation for the surface layer is the one-dimensional dispersive flow equation with crossectionally averaged variables:

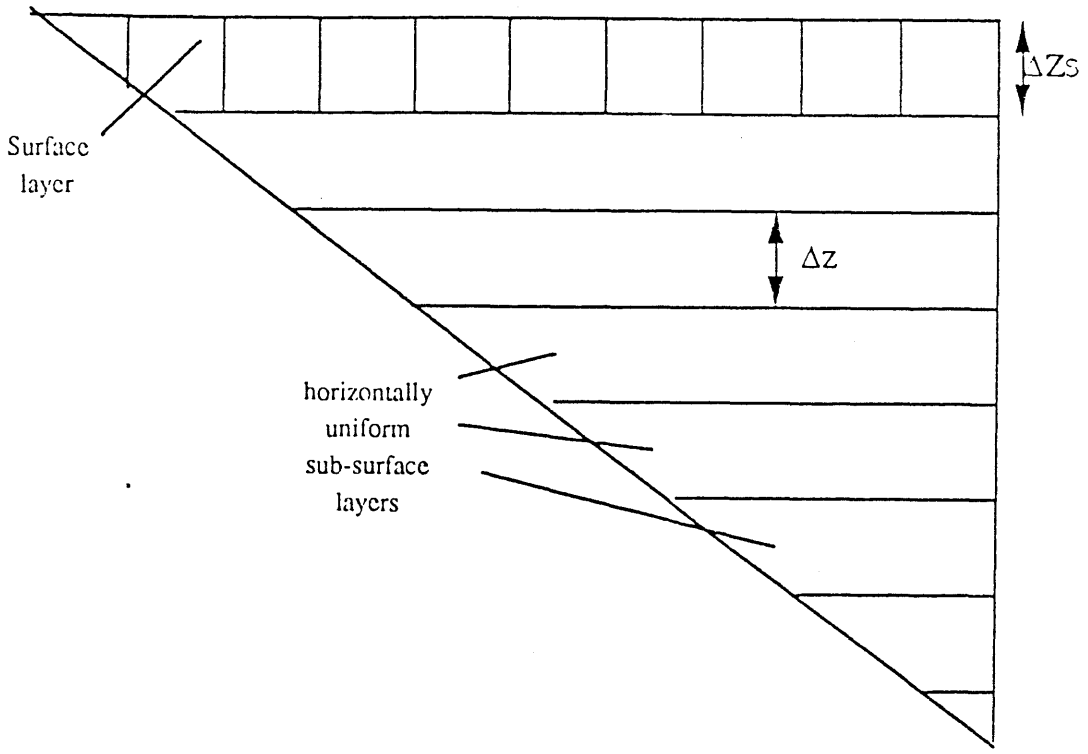

Figure 2-1 Schematic of a deep stratified cooling pond

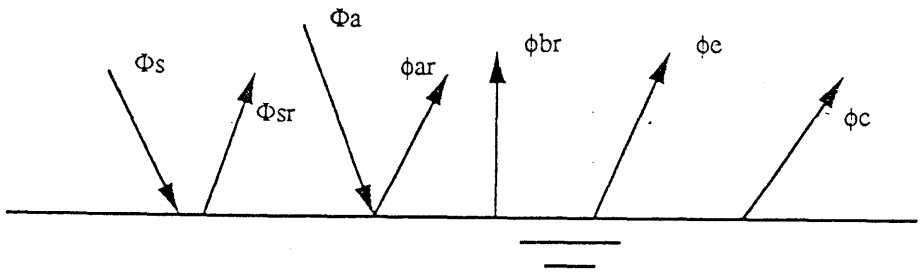

Figure 2-2 Components of surface heat transfer

$$\frac{\partial T}{\partial t} + U\frac{\partial T}{\partial x} = E_L\frac{\partial^2 T}{\partial x^2} + \frac{\phi_n}{\rho c H} \tag{2.1}$$

where T is the crossectional mean temperature, $U = (Q_0 D_v)/A_x$ is the crossectional mean velocity, x is the longitudinal distance, Q_0 is the plant discharge rate, A_x is the vertical crossectional area of the element, t is time, E_L is the longitudinal dispersion coefficient, H is the mean depth of the layer, ϕ_n is the net heat flux across the surface (positive into the water), and ρc is the specific heat per unit volume, which is assumed constant. The flow downwells into the lower layer at the end of the surface layer. The boundary conditions are:

At the upstream side (end of the entrance mixing region):

$$T\Big|_{x=0} + \frac{E_L}{U}\frac{\partial T}{\partial x}\Big|_{x=0} = T_m \tag{2.2}$$

At the downstream side (downwelling):

$$\frac{E_L}{U}\frac{\partial T}{\partial x}\Big|_{x=L} = 0 \tag{2.3}$$

The method used to estimate D_v follows after Jirka et al. (1978) and is outlined in the appendix.

2.1.2 Hypolimnion

For the hypolimnion, the governing equation is the one-dimensional vertical model

$$\frac{\partial T}{\partial t} + \frac{1}{A}\frac{\partial}{\partial z}(Q_v T) = \frac{D_z}{A}\frac{\partial}{\partial z}\left[A\frac{\partial T}{\partial z}\right] + \frac{Bu_i T_i}{A} - \frac{Bu_0 T}{A} - \frac{1}{\rho c A}\frac{\partial}{\partial z}(A\phi_z) \tag{2.4}$$

where T is the temperature at depth z, A is the horizontal area of the element, B is the element width, u_i is the horizontal inflow velocity, T_i is the inflow temperature, u_0 is the horizontal outflow velocity, Q_v is the vertical flow rate, ϕ_z is the internal short wave solar radiation per unit horizontal area, and D_z is the vertical diffusion coefficient. Jirka et al. (1978) state that in the hypolimnion, the vertical transport of heat by advection is often large enough to dominate the transport of heat by diffusion, especially when the intake from the reservoir is deep (as is the case at Mount Storm Lake). By non-dimensionalizing the governing heat transport equation (Eq. (2.4)), they were able to show that the predicted temperature profiles are relatively insensitive to the value of the turbulent diffusivity within the range of one to one hundred times the molecular value (~0.0125 m^2/day) for reservoirs with significant flowthrough. In simulating Mount Storm Lake, it is assumed that the vertical diffusion coefficient is a constant 1.29 m^2/day, with depth.

The incoming solar radiation (insolation) at any depth z, ϕ_z can be described by the equation

$$\phi_z = (1 - \beta)\phi_{sn}e^{-\eta z} \tag{2.5}$$

where β is the long-wave portion of the incoming insolation (which is absorbed near the surface); η is the extinction coefficient of solar radiation in water; and ϕ_{sn} is the net solar heat flux into the water body (incident minus reflected). Values of η and β can be obtained from field measurements. β is typically in the range 0.4 to 0.5 and the value used in modeling Mount Storm Lake is 0.5. η is related to the Secchi disk depth, d_D, by the formula

$$\eta = 1.7/d_D(\text{meters}^{-1}) \tag{2.6}$$

Field measurements at Mt. Storm Lake show d_D in the range of 1 to 4 m, but model results show little sensitivity in the corresponding range of η from 1.5 to 0.3 m^{-1}.

The horizontal velocities are computed from inflow and outflow rates while vertical velocities are computed from the continuity equation for each element

$$Q_v(z,t) = B\left[\int_0^z u_1(z,t)dz - \int_0^z u_0(z,t)dz\right] \tag{2.7}$$

The boundary conditions are:

Surface Boundary Condition:

$$D_z\frac{\partial T}{\partial z} = \phi_n \quad \text{at} \quad z = z_s \tag{2.8}$$

Bottom Boundary Condition:

$$\frac{\partial T}{\partial z} = 0 \quad \text{at} \quad z = 0 \tag{2.9}$$

It is assumed that there is no heat flux to or from the earth through the bottom or sides of the lake (Ho et al., 1984).

2.1.3 Estimation of the Net Heat Flux

A great deal of empiricism is involved in the estimation of the net surface heat flux across a water surface. This is due to the fact that a large number of physical processes govern the flux; also, an extensive and typically unavailable amount of data is required to account for these processes individually (Jirka et al., 1977). The formulae applied in MITEMP follow those recommended by Ryan et al. (1974),

which have been used extensively for predictions of cooling pond behavior with generally good results (Adams et al., 1987; Helfrich et al., 1982; Octavio et al., 1980).

The net heat flux ϕ_n is made up of several terms. The major processes considered (see Figure 2.2) are solar and atmospheric radiation, back radiation, evaporation, and conduction. The net heat influx is defined as

$$\phi_n = \phi_{sn} + \phi_{an} - \phi_{br} - \phi_e - \phi_c \tag{2.10}$$

The net shortwave solar radiation, ϕ_{sn}, is the difference between the incident and reflected solar radiation. The incident shortwave radiation comes primarily from the sun, and is absorbed by gases of the air, water vapor, clouds, and dust as it passes through the earth's atmosphere. The net shortwave radiation may be evaluated either by direct measurement which is the most accurate approach or by indirect evaluation using suitable easily measurable quantities. (Empirical formula used to estimate this flux are provided by Wunderlich (1972), Kasten (1964), among others). When daily averaged values are sufficient, Ryan et al. (1974) recommend the empirical curves by Hamon et al., (1954). These curves are based on data from 20 weather stations throughout the U.S. and give daily averaged insolation as a function of latitude, day of year, and percent of possible sunshine. The incident solar radiation may be obtained by modifying the clear sky radiation obtained from the curve as follows (Adams et al., 1981):

$$\phi_s = (1 - 0.65\dot{C}^2)\phi_{sc} \tag{2.11}$$

where C is the cloud cover (expressed as a fraction) and ϕ_{sc} is the clear sky solar radiation obtained using the 100% possible sunshine curve.

The reflected radiation may be expressed as a fraction of the incident radiation. Using data obtained from the Lake Hefner study, Ryan and Harleman (1973) suggest 6% reflection, so that the net shortwave solar radiation is given as

$$\phi_{sn} = 0.94(1 - 0.65C^2)\phi_{sc} \tag{2.12}$$

The net atmospheric radiation, ϕ_{an}, is the long-wave radiation emitted by water vapor, carbon dioxide, and ozone. This flux may also be measured or computed as a function of the air temperature. The basic equation for the incident atmospheric radiation, ϕ_a, is given as

$$\phi_a = \epsilon\sigma T^{*4} \tag{2.13}$$

where ϵ is the average emittance of the atmosphere, σ is the Stefan Boltzmann constant, and T^* is the air temperature (°K, absolute).

Most formulae for atmospheric radiation were developed for a clear sky and then modified for cloud cover. Clouds tend to darken the atmosphere, thus increasing its emissivity. A value of 3% is generally accepted for the reflectance or albedo of a water surface to longwave radiation (Jirka et al., 1977). Using the clear sky formula of Swinbank (1963) the net longwave atmospheric radiation is thus

$$\phi_{an} = 0.97\phi_a = 1.06 \times 10^{-11} \times (T_a + 273.16)^6(1 + 0.17C^2) \tag{2.14}$$

where ϕ_{an} is in kcal/m^2-d and T_a is the air temperature in °C.

The long-wave back radiation from the water surface ϕ_{br} is the largest single item in the energy budget and is a function of the water surface temperature. In units of Kcal/m^2-d it may be calculated as

$$\phi_{br} = 1.14 \times 10^{-6}(T_s + 273.16)^4 \tag{2.15}$$

where T_s is the water surface temperature in °C. This component of the surface heat flux is the most accurate because the emissivity of water (~97%) is fairly well known.

The evaporative heat flux ϕ_e is the product of the latent heat of evaporation and the rate of evaporative mass transfer across the air-water interface. For water bodies with artificial heat loading, this flux is made up of two components: free convection and forced convection. Free convection is the transport of water from the water surface to the atmosphere as a result of buoyancy effects. For heated water bodies, it is calculated as a function of the virtual temperature which includes the effects of temperature and water vapor content. (The virtual temperature is defined as the temperature dry air would have if its pressure and density were the same as those of the moist air.) Forced convection is due to wind effects. The equation used in MITEMP follows Ryan et al. (1974) as calibrated by recent MIT experience (Helfrich et al., 1982; Adams et al., 1987). In units of Kcal/m^2-d,

$$\phi_e = 0.85(2.712)\left[22.4(T_{vs} - T_{va})^{\frac{1}{3}} + \frac{W}{0.447}\right](e_s - e_a) \tag{2.16}$$

where W is the wind speed in m/s; T_{vs}, T_{va} are the virtual temperatures of the water surface and the air respectively; and e_s, e_a are the saturation vapor pressures at the water surface and in the atmospheric at elevation 2 m respectively in mm Hg.

The conduction flux ϕ_c from the water surface to the atmosphere is related to the evaporative flux through the Bowen ratio. In similar units it is

$$\phi_c = \frac{\phi_e}{0.46}(T_s - T_{air})/(e_s - e_a) \tag{2.17}$$

2.1.4 Solution

The surface layer equation (Eq. (2.1)) is written in finite difference form using the Crank-Nicholson method for time integration. The equations and boundary conditions for the hypolimnion are also written in finite difference form and are solved simultaneously using an explicit time step.

2.2 Application to Mount Storm Lake

2.2.1 Schematization

Mount Storm Lake is schematized in MITEMP as a deep cooling pond. The surface layer depth h_s is obtained from the following expression developed by Watanabe et al. (1975).

$$h_s = \left[\frac{f_i}{4}\frac{Q_0^2}{\beta\Delta T_0 g}\frac{(D_v L)^3}{A_p^2}\right]^{\frac{1}{4}} \tag{2.18}$$

which is equivalent to

$$h_s = \mathbb{P}H \tag{2.19}$$

where $\mathbb{P}$ is the pond number (see Appendix A), H is the mean pond depth, and A_p is the total pond area. Using parameters appropriate for Mt. Storm Lake, $h_s \simeq 2$ m and a constant value of 2 m was used in all model simulations. The hypolimnion is divided into sixteen layers each with a thickness also of 2 m.

In deep stratified cooling ponds, temperature variations during the day are limited to diurnal fluctuation in the surface layer. To avoid these diurnal effects, a time step of one day was chosen. This effectively captures the transient nature in terms of seasonal differences and day-to-day variability without the influence of fluctuations during the day.

2.2.2 Input Data

The input requirements to the model are of three types: the meteorological data, the pond geometry data, and the initial temperature structure of the pond.

The meteorological data include the daily mean air temperature, wind speed measured at 2 m above the water surface, dewpoint temperature, and cloud cover. Air temperature and wind speeds were obtained primarily from the meteorological station at the site, but when not available, local climatological data (NOAA) were used. NOAA data were also used for dewpoint and cloud cover. The NOAA station chosen is located at Elkins, West Virginia (lat 38°53′N, long 79°51′W), at an elevation of 1948 feet and was the closest NOAA station to Mount Storm Lake (lat 39°12′N, long 79°16′W) which is at an elevation of 3240 feet. The net solar radiation was computed from Eq. (2.12) where the clear sky solar radiation were obtained from the graph by Hamon (1954).

Pond geometry data include the horizontal crossectional area, breadth, and length at each layer, and were obtained using Figure 2.3 and a topographical map of the lake.

The initial temperature structure of the pond was obtained from measurements of vertical temperature profiles taken at the site. The inflow temperatures of heated water were determined by adding the daily averaged condenser temperature rise to the intake temperature. The daily plant operational data (MWh) were converted to daily average condenser temperature rise for input to the model by scaling it with the ratio of the maximum temperature rise to the maximum power output. (See following section.)

2.3 Initial Modifications to the Model

2.3.1 Condenser Temperature Rise

The model MITEMP has the capability to determine the discharge temperatures from one of two methods

i) For closed cycle operation, a daily condenser temperature rise and flow are required. The discharge temperature is computed as the intake temperature plus the condenser temperature rise.

ii) For open cycle generation, the input discharge temperature and flow are used directly.

The operation of Mount Storm Lake may be classified as closed cycle. However, the data available on a daily basis for the simulation consists of the power generated. These data were converted to a condenser temperature rise by assuming a constant (averaged) flow rate as

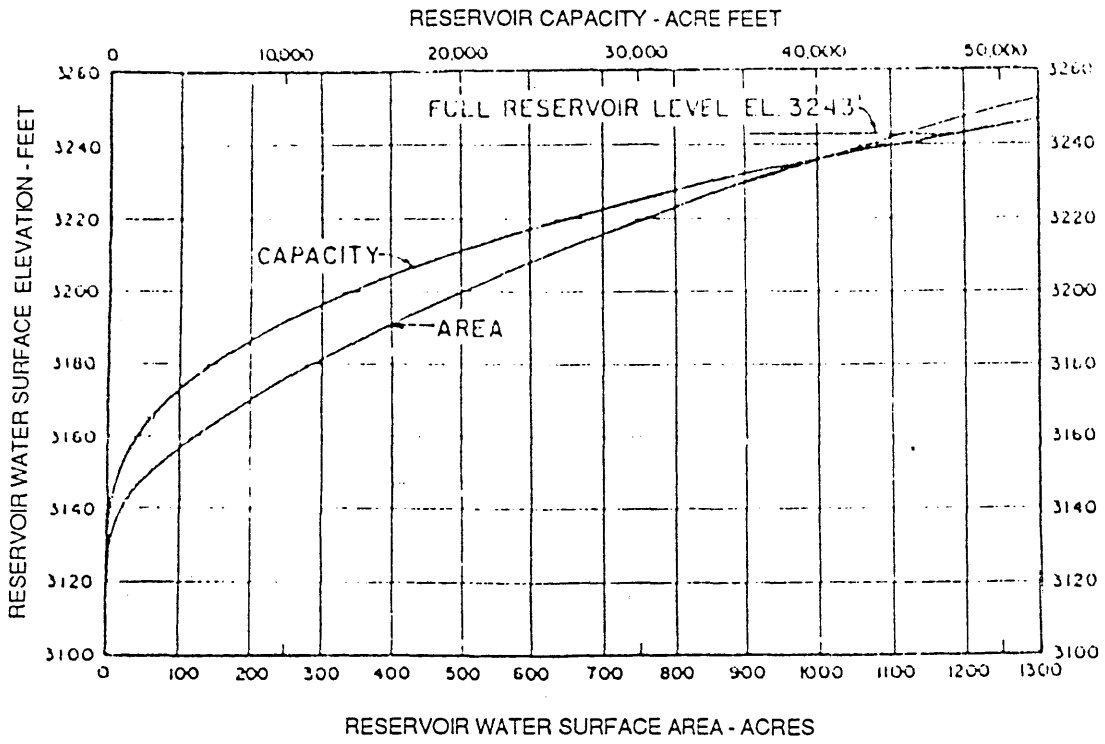

Figure 2-3 Reservoir area and capacity curves

$$\text{temperature rise (in °C)} = \frac{\text{energy generated in 24 h}}{\text{maximum power capacity} \times 24\ \text{h}} \times \begin{bmatrix}\text{max. condenser}\\ \text{temp. rise}\end{bmatrix} \tag{2.20}$$

The maximum condenser temperature rise of 10.2° C was obtained from available data on temperature rise across the condenser when the plant is operating at its full capacity.

2.3.2 Evaporative Heat Flux, ϕ_e

MITEMP estimates the evaporative heat flux from Ryan's equation for a heated lake (see Eq. (2.16))

$$\phi_e = F(W_z)(e_s - e_a) \tag{2.21}$$

where ϕ_e is the heat flux; $F(W_z)$ is the wind speed function based on wind speed measured at height z; e_s is the saturation vapor pressure at the water surface temperature; and e_a is the vapor pressure in the air obtained from

$$e_a = \psi 25.4 \exp\left[17.62 - \frac{9500}{T_a + 460}\right] \tag{2.22}$$

where T_a is the air temperature in °F, ψ is the relative humidity expressed as a fraction, and e_a is in units of mm Hg. For a model time step of one day, MITEMP thus computes the atmospheric vapor pressure using daily averaged relative humidity. However, because of variations in air temperature, the relative humidity is highly variable over the period of a day and as a result, the arithmetic mean of the three-hourly data (three hours is the typical interval provided by NOAA) might not produce a meaningful value. The options were to either use the mean, use all

the data so that the time step for the relative humidity data is three hours, or to use another meteorological variable. The dew point temperature is a much less variable measure of the humidity and therefore the vapor pressure at the air temperature was rewritten in terms of the dewpoint temperature. In equivalent units

$$e_a = 25.4 \exp\left[17.62 - \frac{9500}{T_{dew} + 460}\right] \tag{2.23}$$

where T_{dew} is the dew point temperature in °F.

3 CALIBRATION AND VERIFICATION OF THE 1-D MODEL

The output from MITEMP includes the temperature variation in the epilimnion as well as that in the hypolimnion. A daily time series of temperature at various locations can therefore be obtained as well as temperature profiles in the lake on specific days (the dates for which profiles are desired are specified in the input file).

Model calibration involves the analysis of the model output and the data to evaluate the possibility of improvement of the temperature predictions. The calibration is based on a full year of data (Sept. 1986 - Aug. 1987). The model validation compares the model output from the calibrated model with data for another year (Sept. 1987 - Aug. 1988). It was expected that no model adjustments would be required for the validation.

3.1 Data Collection

The temperature data collection effort was performed on both a continuous and a so-called in-situ basis. Continuous recording consists of daily measurements of the daily maximum and mean temperatures at six stations in the lake as well as daily measurements above the spillway at the dam and below the dam. ENDECO recorders with an accuracy of $\pm 0.2^{\circ}$C were used for this purpose. In-situ temperature monitoring consists of vertical temperature profiles taken at each of the six stations, MSL-1 through MSL-6 (Figure 3.1), during biological surveys in 1987 (May, July, and September) and in 1988 (April - September; there were no data in May due to equipment malfunction). Vertical temperature profiles are also available at times of ENDECO change: October 14, 1987, January 15, 1988, and May 4, 1988. In addition, weekly temperature transect surveys were done during the months of July and August both in 1987 and 1988, at ten locations, A-1 through

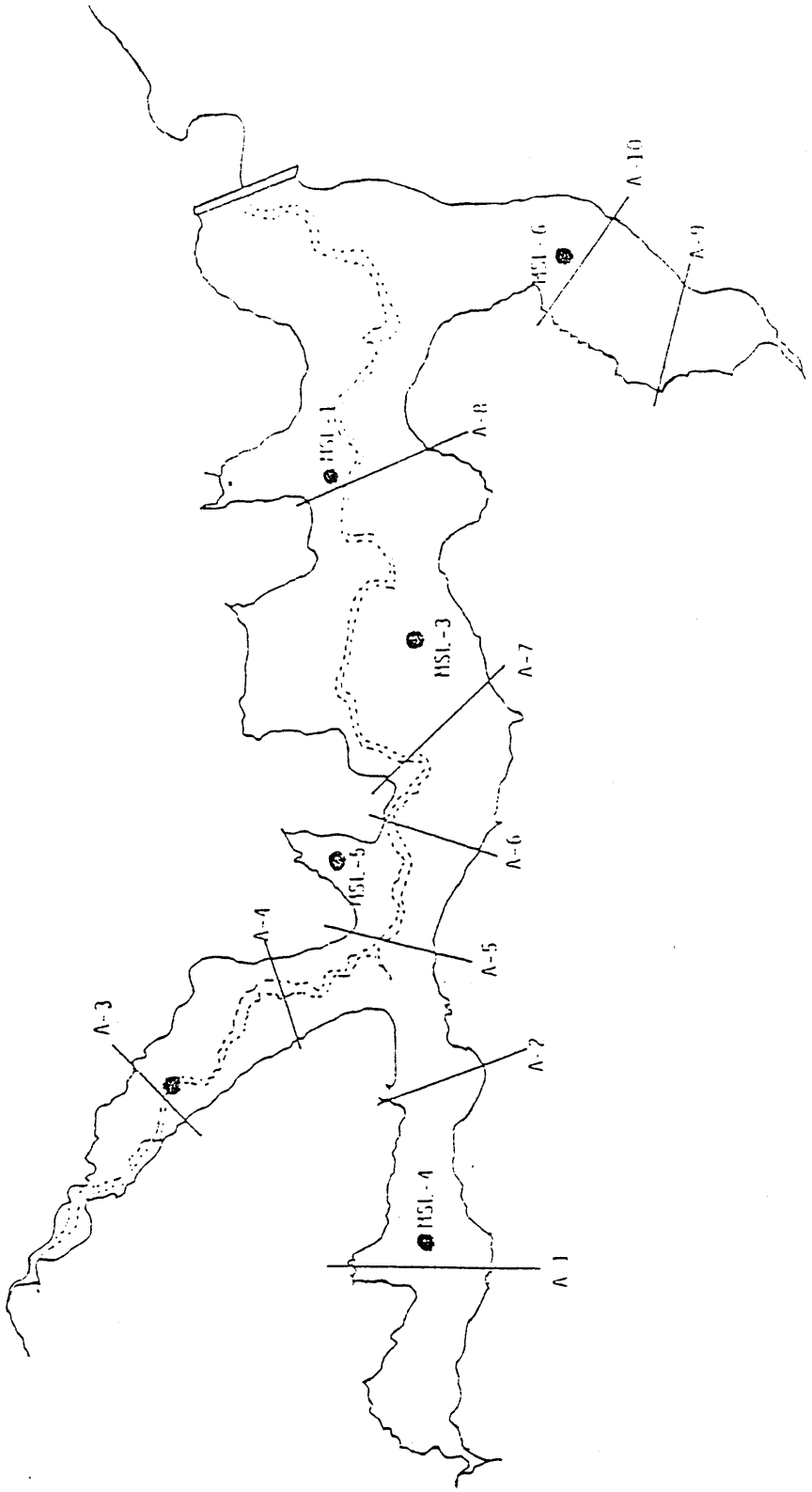

Figure 3-1 Mount Storm Lake summer temperature transects

A-10 (see Figure 3.1). The instruments used in the temperature transect surveys have an accuracy of ±0.1° C.

3.2 Results of the 1-D Model (First-Year Simulation, Sept. 1986 - Aug. 1987)

The output from the model is compared in two ways. The vertical temperature profiles are compared on dates for which vertical profile data are available.

Since the model is horizontally uniform in the hypolimnion, the predicted profiles vary only in the epilimnion. Therefore, the comparison of the profiles against measurements included both the maximum and minimum predicted surface temperatures as bounds. See Figures 3.2-3.8. On average the profiles look quite good. Some observations that may be made from the figures are:

i) There may be a lag in the model's response; the predicted temperature profiles increase in temperature from May to July and then decrease. Although this is consistent with the observed data (see Figure 3.9), the model is underpredicting (or lagging) the measurements in early July (see Figures 3.3, 3.4) and increases gradually through August. However it is difficult to be conclusive using only two months (July and August) of data.

ii) In most of the plots (see Figure 3.4-3.8) the temperature drop across the epilimnion in the model is slightly higher than in the measurements. This may be a result of using insufficient entrance mixing which produces a high initial temperature.

iii) For the most part, it appears that the 1-D model captures the vertical structure in the cooling lake. Note that the measured profiles are fairly uniform spatially; the

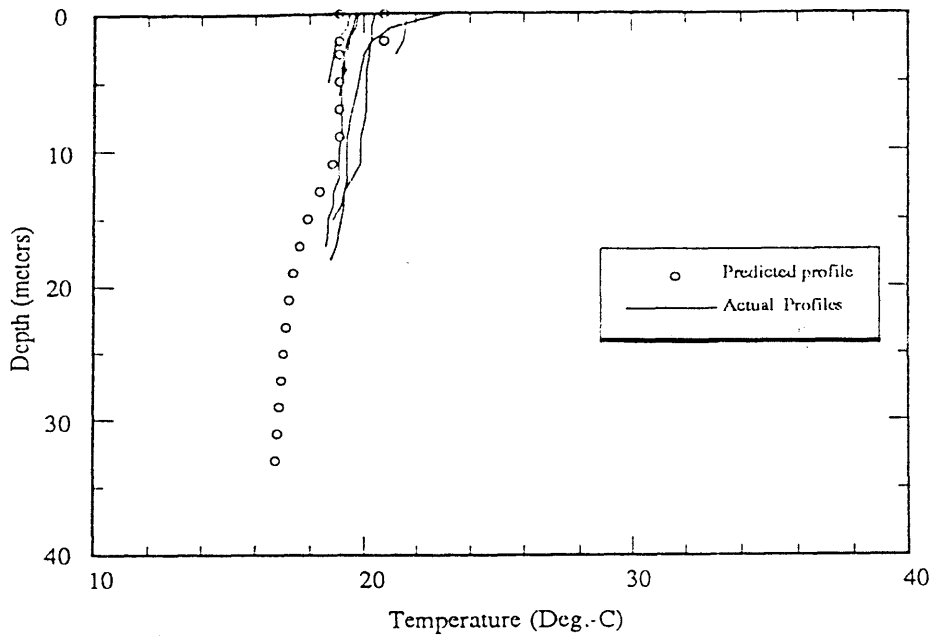

Figure 3-2 Measured and predicted temperature profiles for May 14, 1987

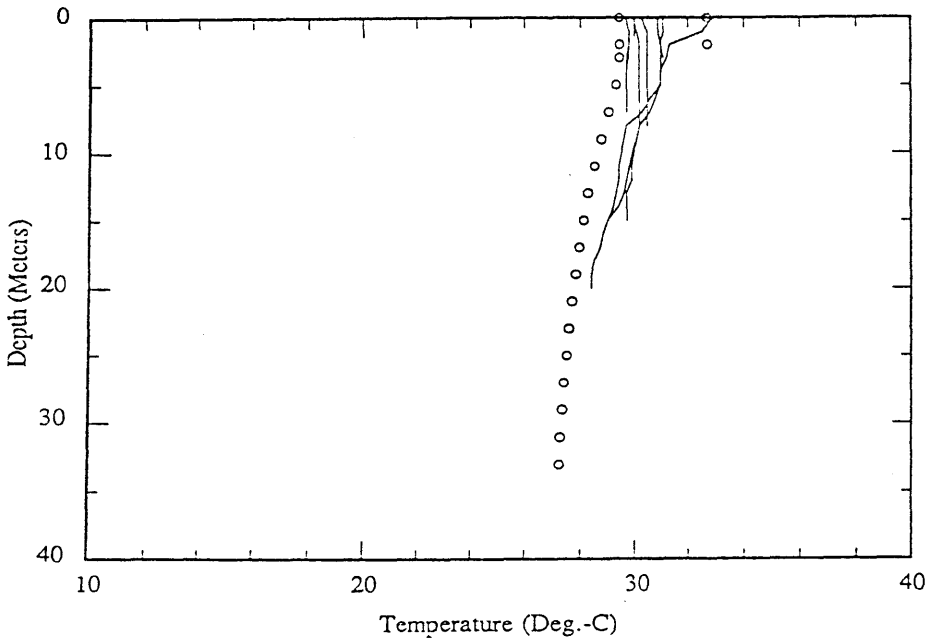

Figure 3-3 Measured and predicted temperature profiles for July 7, 1987

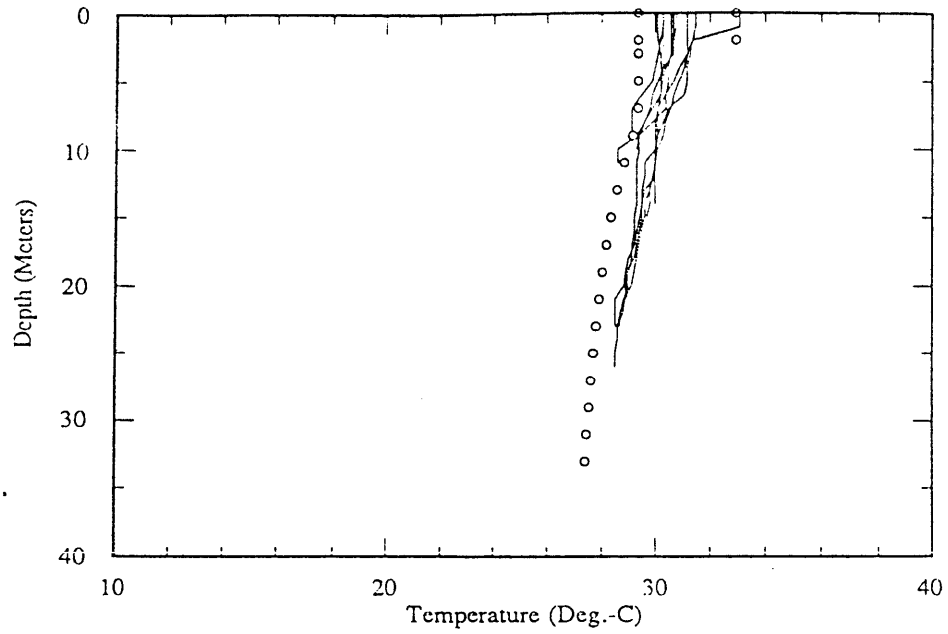

Figure 3-4 Measured and Predicted Temperature Profiles for July 8,1987

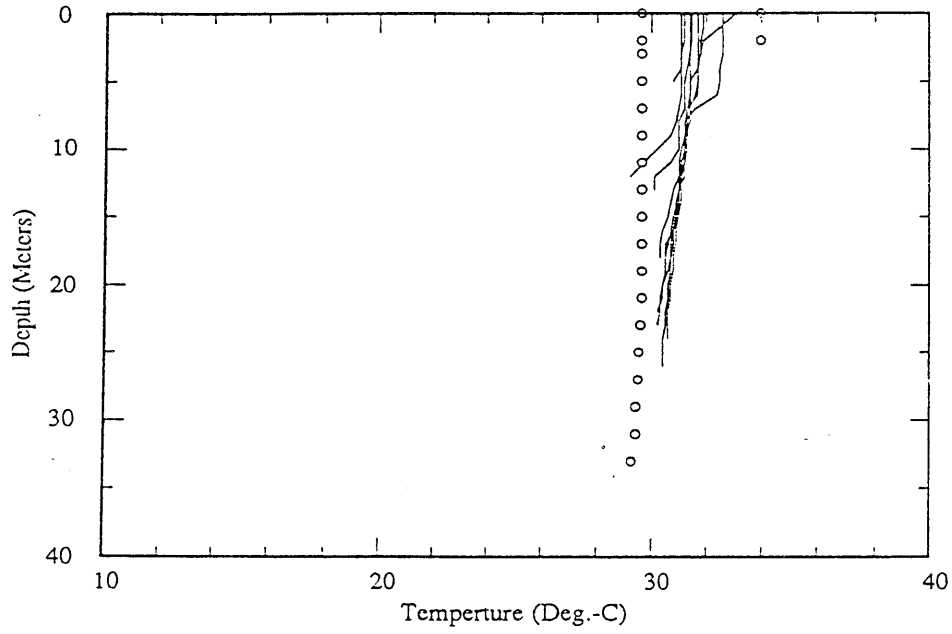

Figure 3-5 Measured and predicted temperature profiles for July 16, 1987

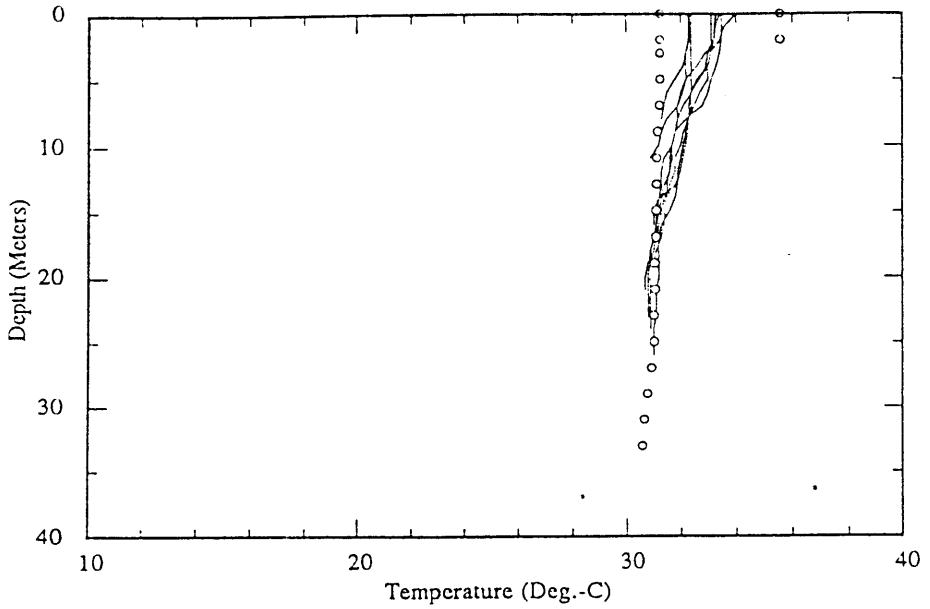

Figure 3-6 Measured and predicted temperature profiles for July 30, 1987

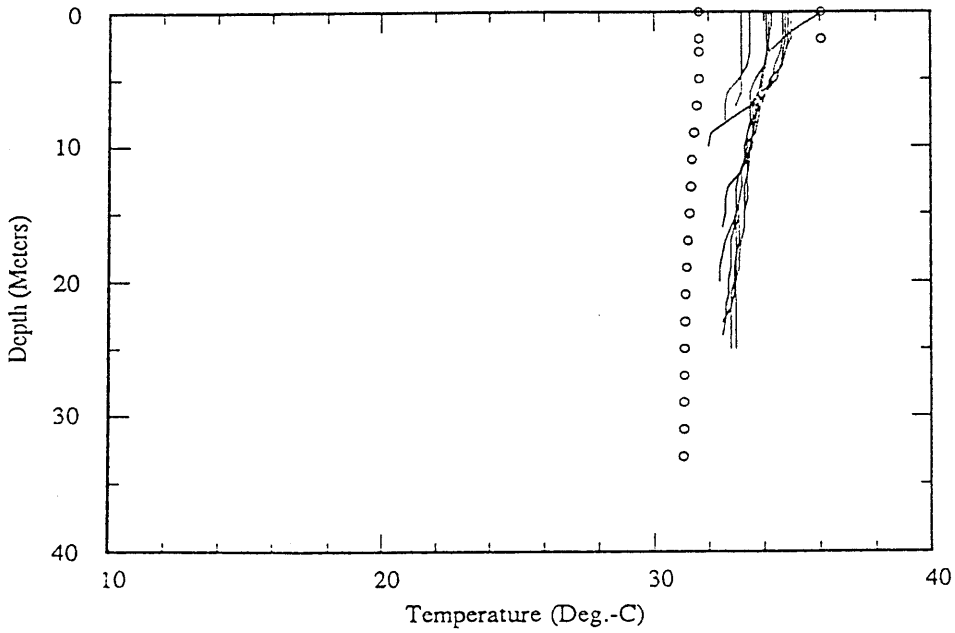

Figure 3-7 Measured and predicted temperature profiles for August 3, 1987

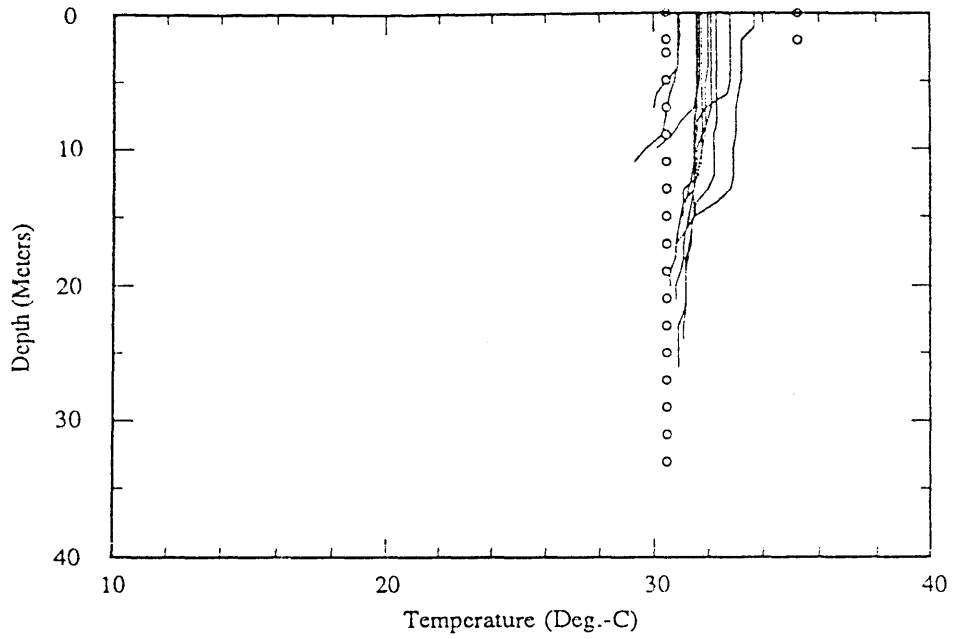

Figure 3-8 Measured and Predicted Temperature Profiles for Aug 28, 1987

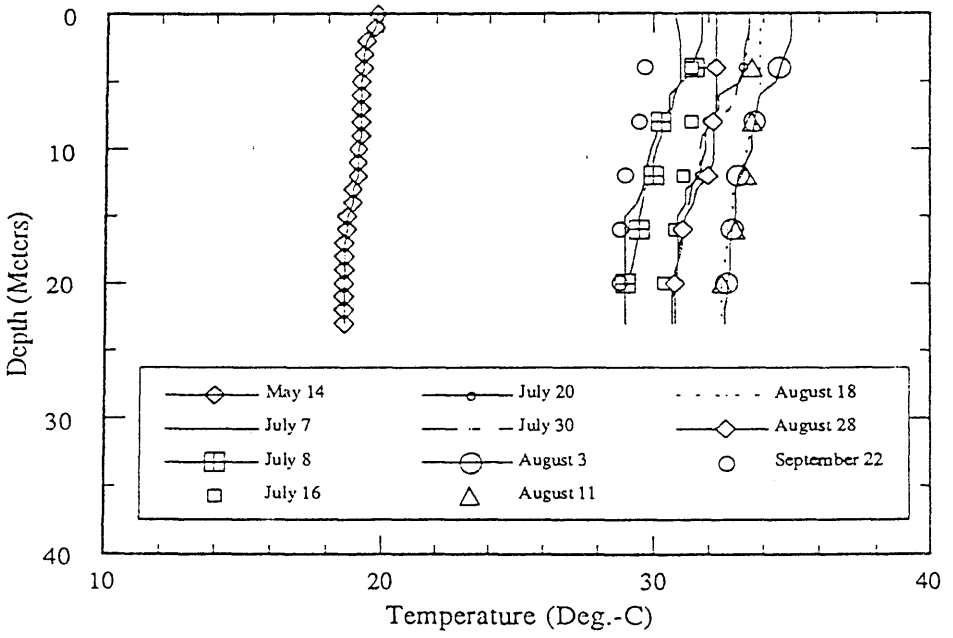

Figure 3-9 Mt. Storm Lake Observed Temperature Profiles
May - September 1987
(At transect A - 7 & MSL - 3)

horizontal range in the hypolimnion is always less than 2° C. This supports the use of the 1-D model.

Also, the daily temperature time series obtained from the model are compared with the continuous data observed at three locations chosen to evaluate the model's performance.

The locations at which the time series were compared are

i) Near the discharge (the maximum surface temperature). The observed surface temperature at MSL-1 (see Figure 3.1) is compared to the temperature in the first model segment of the epilimnion.

ii) The minimum surface temperature within the main region of the lake (excluding the upstream side arms associated with Stony River and Helmick Run). The observed surface temperature at MSL-5 is compared to the temperature at the end of the fifth model segment of the epilimnion.

iii) The bottom temperature. The observed bottom temperature at MSL-1 is compared to the predicted temperature in the fifth horizontal layer above the bottom, that is at a depth of about 23.5 m.

The differences between predicted and observed time series at each of these locations are shown in Figure 3.10a-c. The mean error over the year at each of the locations was between 0° C and -1.1° C (see Table 3.1).

From Figure 3.10 and Table 3.1 the main differences between prediction and measurements may be summarized as follows

a) Max. surf. temp. diff. (pred - obs)

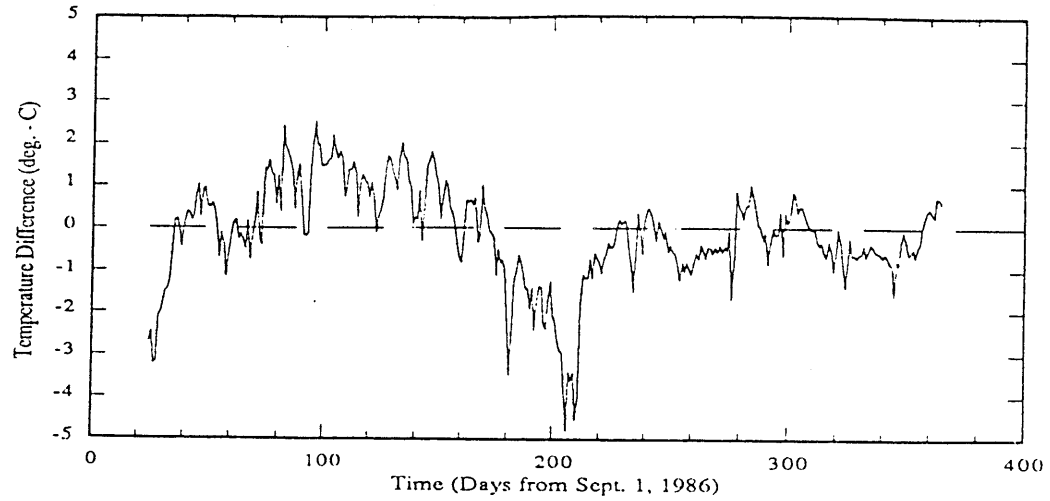

b) Bot. temp. diff. (pred. - obs)

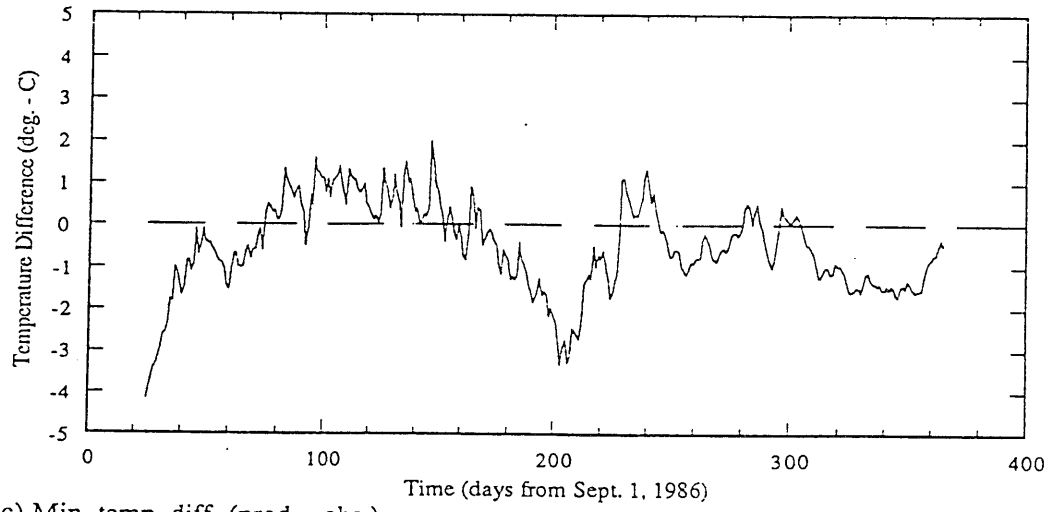

c) Min. temp. diff. (pred. - obs.)

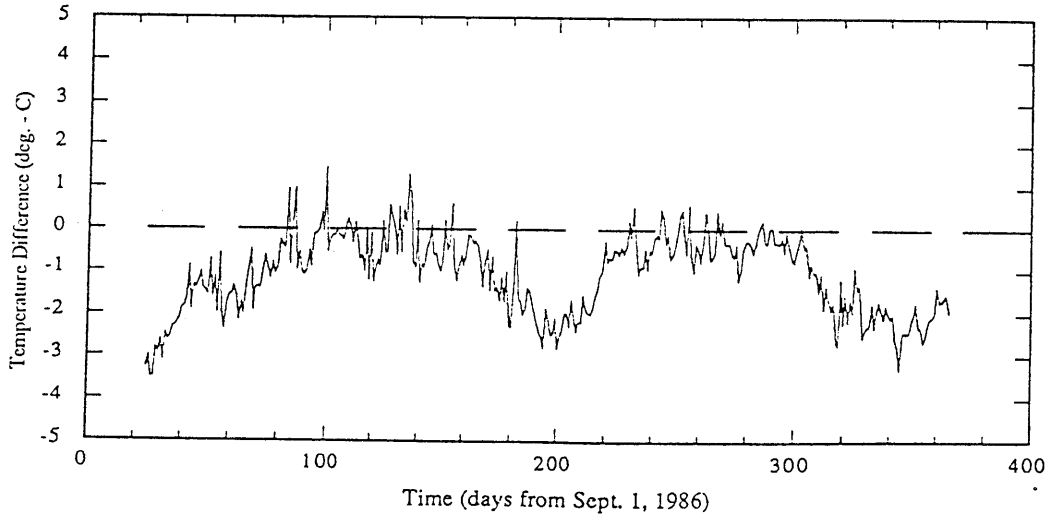

Figure 3-10 Time Series of Temperature Differences
First Simulation Year (Sept. 1986 - Aug. 1987)

Table 3.1

Error Statistics of Time Series for First-Year Simulation (Sept. 1986 - Aug. 1987)

	Mean			Std. Dev.		
	Pred	Obs	Diff	Pred	Obs	Diff
MSL-1 (surface)	22.47	22.52	-0.14	7.52	7.76	1.19
MSL-1 (bottom)	18.74	19.14	-0.52	7.15	7.71	1.08
MSL-5 (surface)	19.60	20.49	-1.07	7.26	7.78	0.94
avg			-0.58			

i) If the temperature drop across the epilimnion from MSL-1 to MSL-5 is defined as ΔT then the temperature drop in the model (predicted) and in the lake (measured) are

$$\Delta T_p = P_{max} - P_{min} \tag{3.1}$$

$$\Delta T_m = M_{max} - M_{min} \tag{3.2}$$

respectively, where P_{max}, P_{min} are the maximum and minimum surface temperatures in the model and M_{max}, M_{min} are the maximum and minimum measured temperatures respectively. Using averages from Table 3.1,

$$P_{max} - M_{max} = -0.1 \tag{3.3}$$

$$P_{min} - M_{min} = -1.1 \tag{3.4}$$

$$P_{max} - P_{min} = M_{max} - M_{min} + 1.0 \tag{3.5}$$

Or,

$$\Delta T_p = \Delta T_m + 1.0 \tag{3.6}$$

This gives the same conclusion obtained from looking at the vertical profiles: the horizontal temperature drop across the epilimnion in the model is more than the observed temperature drop.

ii) The model consistently underpredicts (slightly) the data at all three points but more so at the lake bottom.

iii) There appears to be some seasonality in the difference (pred. - obs.). The difference is a little higher than average during the fall/winter season and a little lower during the spring suggesting a possible phase lag in the model's response.

iv) Table 3.1 indicates that the error in the prediction of the bottom temperatures is more than at the surface at MSL-1 by about 0.3° C. This could be due to either insufficient vertical diffusion of heat below the surface layer or insufficient heat input to the model.

3.3 Calibration of the 1-D Model (First-Year Simulation)

The possible causes of the small differences described in the previous section were assumed to be due either to

i) Insufficient seasonal distribution of the heat input to the model

ii) Insufficient mixing

Since the most sensitive meteorological parameters—air temperatures and wind speeds—were obtained directly from the Mount Storm Lake station, the next most likely source requiring adjustment is the solar radiation. Solar radiation data were available at the site for only nine months (from June 1987 - February 1988). Figure 3.11 shows the calculated and observed solar radiation. The upper and lower limits are the bounds for clear and cloudy skies using the curves by Hamon et al. (1954). A comparison of this data with the calculated solar radiation, shows that the prediction is generally very close but is about 17% lower on average than the site measurements.

According to Jirka et al. (1978) a major sensitivity for the temperature response is the vertical entrance dilution D_v. Therefore, the primary sensitivity analysis was performed with D_v. Jirka et al. (1978), however, also added that the dispersion coefficient E_L has some effect on highly transient pond characteristics such as plant-induced heat fluctuations. Therefore the sensitivity to the longitudinal dispersion coefficient was also considered.

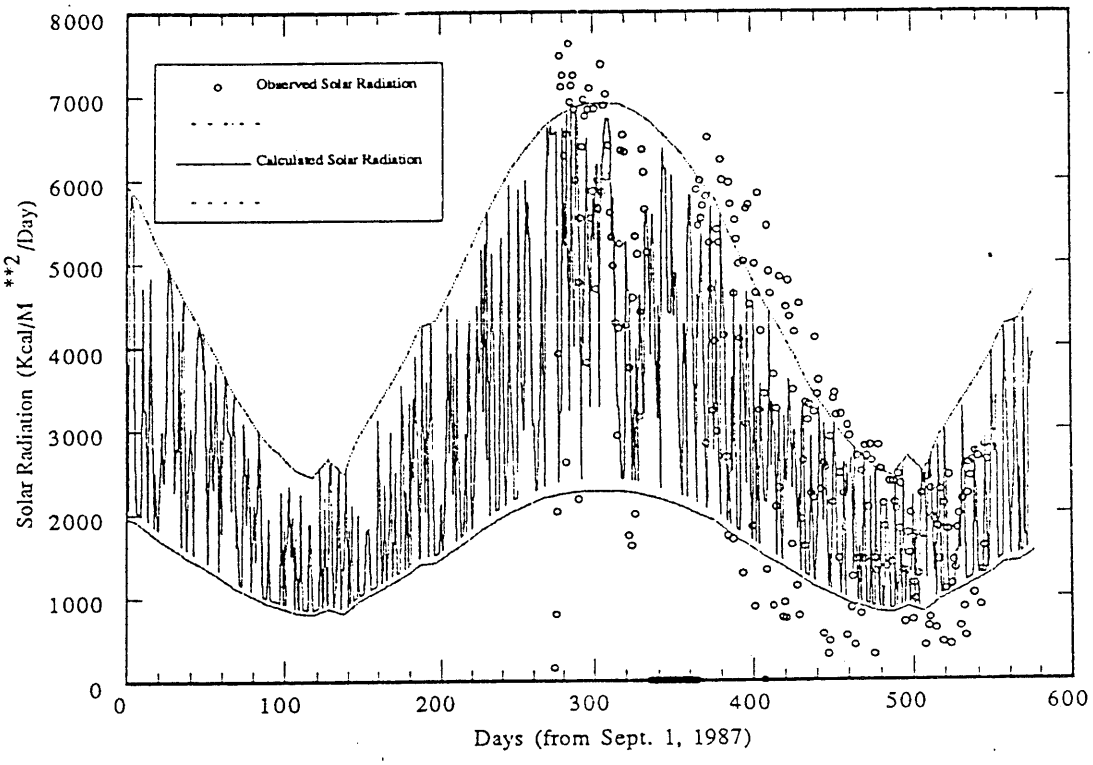

Figure 3-11 Comparison of observed and calculated solar radiation

Finally, a comparison of the residual time series errors with the station generation showed a very significant correlation at all three locations. The time series of the station generation is compared with the errors at MSL-1 (surface) in Figure 3.12a and 3.12b. The possibility of reducing this correlation was also examined.

3.3.1 Correction to Solar Radiation

Figure 3.13 shows the difference between the measured solar radiation and the prediction averaged over each of the nine months for which data are available. The data are summarized in Table 3.2 The errors appear to be periodic about the mean difference with a period of about a year. Therefore reducing this error might eliminate the errors described in b) and c) of Section 3.2.

From Figure 3.13, it may be observed that the error about the mean difference may be approximated by a sine function, that is.

$$E(t) = E^* \sin(\omega t + \phi_e) \tag{3.7}$$

where E^* is the amplitude of the error and ϕ_e is the phase lag. Since only nine months of data are available, a Fourier analysis can not be performed using solar radiation data because at least a full period (in this case one year) of data is required. However, an estimate of E^* and ϕ_e can be determined from Figure 3.13. If a sine curve were drawn through the points, then the difference between the peaks is equal to twice the amplitude, i.e.,

$$2E^* = 1224 \text{ kcal/m}^2\text{/day} \tag{3.8}$$

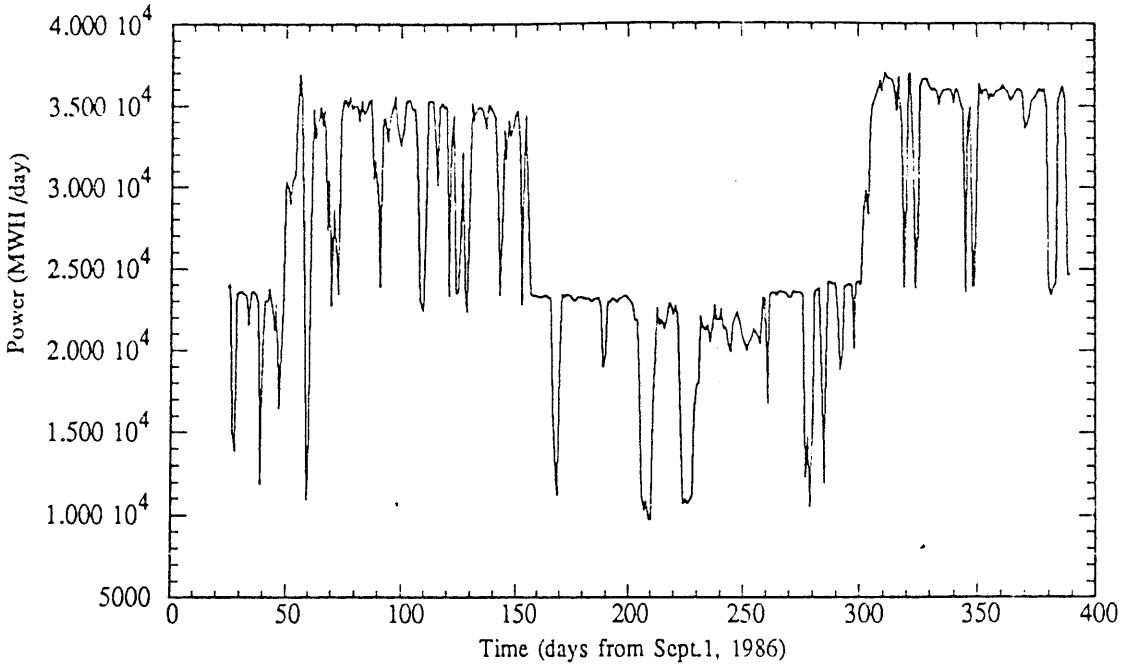

Figure 3-12a Time series of Mount Storm Station power generation

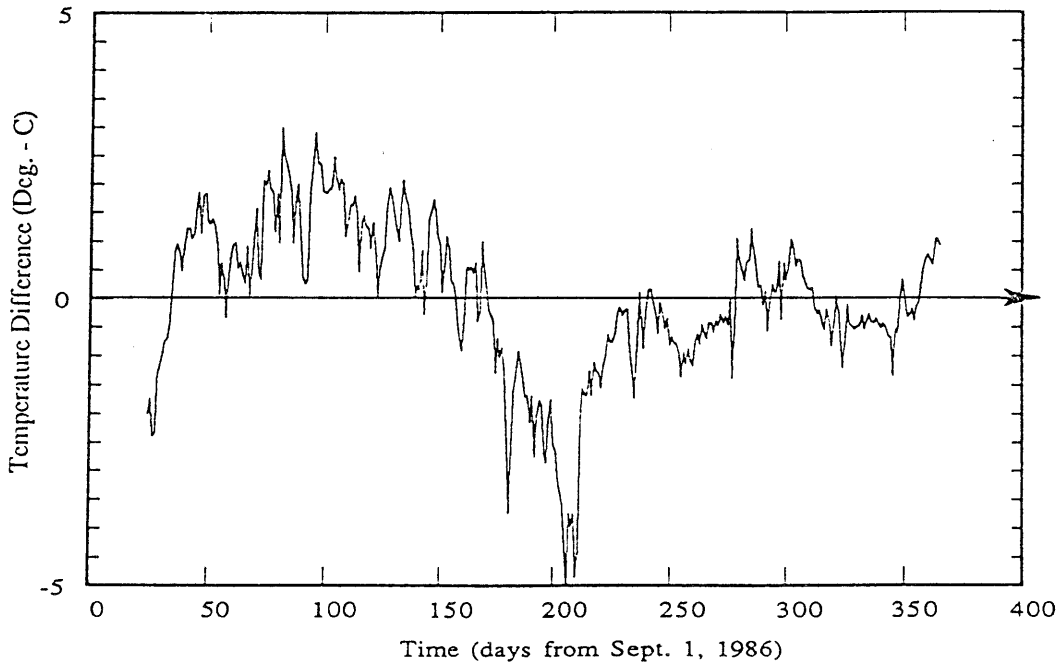

Figure 3-12b Time series of errors at MSL-1 (surface) first simulation year

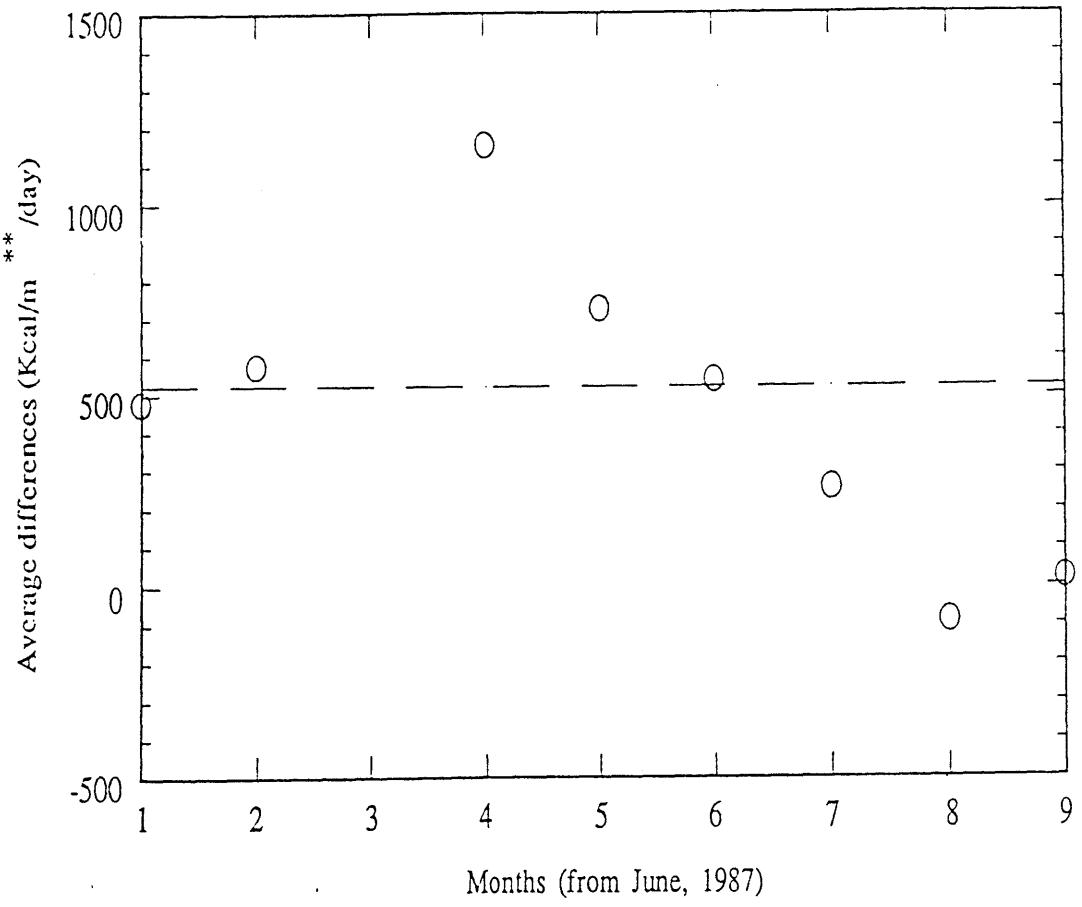

Figure 3-13 Monthly averaged differences in solar radiation (obs. - pred.)

Table 3.2

Monthly Averaged Differences
between Observed and Calculated Solar Radiation Data (in Kcal/m^2/day)

Month	Avg
June	477.15
July	575.26
Sept	1154.56
Oct	727.44
Nov	540.04
Dec	257.29
Jan	-89.40
Feb	20.41
Mean	458.86

Also, since the simulation year starts in September, it appears that the error lags behind the measurements by about three months which is a quarter of a period.

To determine the mean difference to add to the calculated solar radiation, we note that since the monthly errors are periodic, the mean over nine months would be biased. Using the same reasoning described above, the mean difference would lie half way between the peaks or be about 532 kcal/m^2/day. Therefore an error term,

$$E(t) = 532 + 622\sin\left[\frac{2\pi t}{365.25} + \frac{\pi}{2}\right] \tag{3.9}$$

where t is the time in days (beginning in September) and E(t) in Kcal/m^2/day was added to the predictions. The mean error in the solar radiation (see Table 3.3) was reduced from 17% to less than 6% of the measured solar radiation. In addition, the range of the mean error is reduced from over 1000 Kcal/m^2/day to about 500 Kcal/m^2/day. The effect of this calibration is summarized in Table 3.4 for the time series of predicted temperatures (for the first-year simulation). The major conclusion that may be made from this observation is that the initial negative errors (see Table 3.1) were due largely to the insufficient seasonal solar radiation input.

In conclusion, the predictive accuracy of the model is improved by calibrating the calculated solar radiation using solar radiation measurements. The predicted solar radiation data obtained using the curves by Hamon (1954) were increased by adding a constant term and a periodic term. The increase in solar radiation input to the model resulted in a decrease of the mean error of the time series over the three locations from -0.58° C to 0.03° C.

Table 3.3

Calibrated Monthly Averaged Differences between Calculated and Observed Solar Radiation Data ($kcal/m^2$-d)

Month	Avg.
June	-217
July	-394
Sept	31
Oct	-230
Nov	-140
Dec	-104
Jan	-174
Feb	85
Mean	-146

Table 3.4

Error Statistics after Calibration of Solar Radiation for First-Year Simulation

	Mean			Std. Dev.		
	Pred	Obs	Diff	Pred	Obs	Diff
MSL-1 (surface)	23.08	22.52	0.47	7.79	7.79	1.38
MSL-1 (bottom)	19.35	19.14	0.09	7.42	7.71	1.15
MSL-5 (surface)	20.21	20.49	-0.47	7.51	7.78	0.93
Average			0.03			

3.3.2 Effect of Longitudinal Dispersion

The base case calculations use an expression for estimating the longitudinal dispersion E_{LF} within the upper layer derived by Fischer (1967):

$$E_{LF} = 0.3\frac{U_* \ell^2}{\kappa^2 R_h} \tag{3.10}$$

where U_* is the shear velocity ($\sqrt{f/8}U$), f is the friction factor, ℓ is a characteristic transverse length (the lateral distance from the maximum surface velocity to the most distant bank $\simeq$ W/2), κ is the von Karman constant $\simeq$ 0.4, and R_h is the hydraulic radius ($\approx h_s$, the surface layer depth). Using parameters specific to Mount Storm Lake, the magnitude of E_{LF} is about 140 m^2/s. Since the longitudinal temperature distribution is predominantly a function of the dispersion coefficient, this property was used to evaluate what fraction of the Fischer estimate E_{LF} produced the best match between the predicted longitudinal profiles and the measured temperatures. Actual longitudinal temperature profiles were not available but were estimated from the observed temperature time series at stations MSL-1, MSL-3, MSL-5, and MSL-4. A value of 0.25 times the Fischer relationship was found to provide the best match. This result agrees with previous calibration of E_{LF} to cooling lakes (Helfrich et al., 1982; Luxenberg et al., 1986). Figures 3.14a and 3.14b show typical results on different days.

3.3.3 Dilution/Entrainment Factor.

The dilution coefficient in MITEMP determines how much water mixes initially with the heated discharge. Large entrance mixing implies lower peak temperatures and lower rates of heat loss. The base case described above used an initial value of dilution = 2.0. However using parameters for Mount Storm Lake, a theoretical

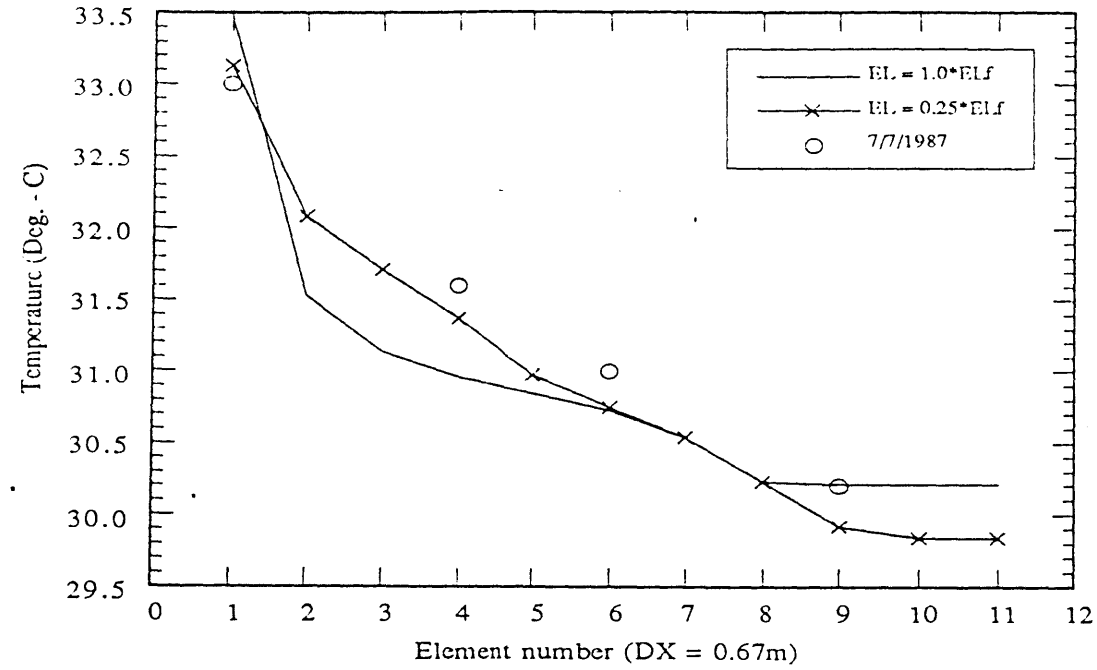

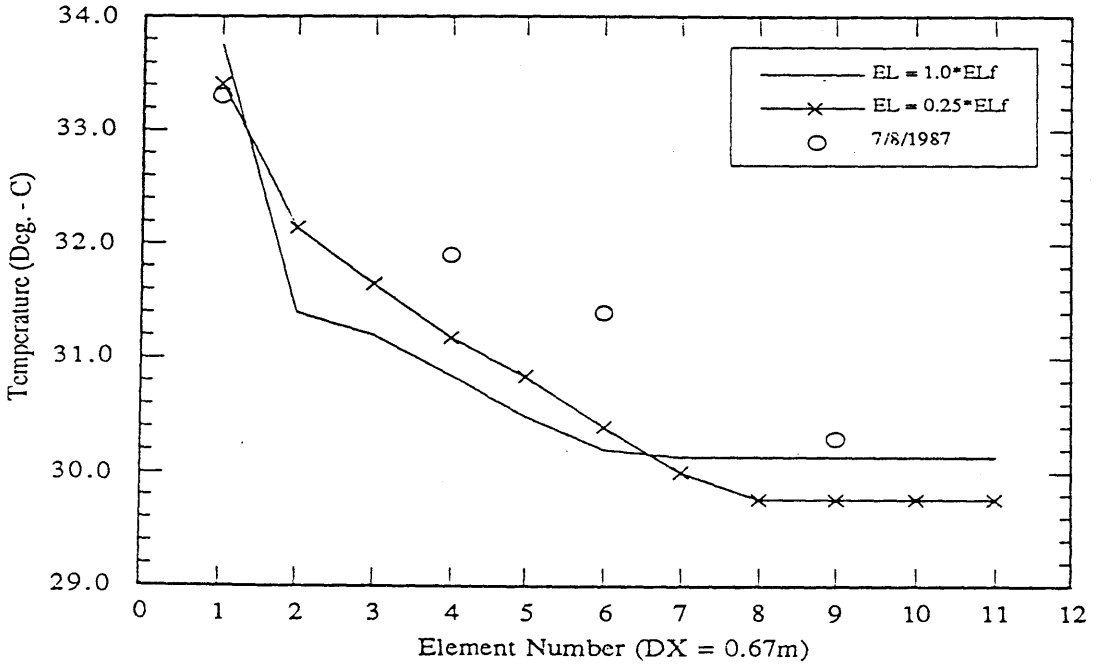

Figure 3-14a Surface temperature variation in Mount Storm Lake as a function of longitudinal dispersion (7/7/87 and 7/8/87)

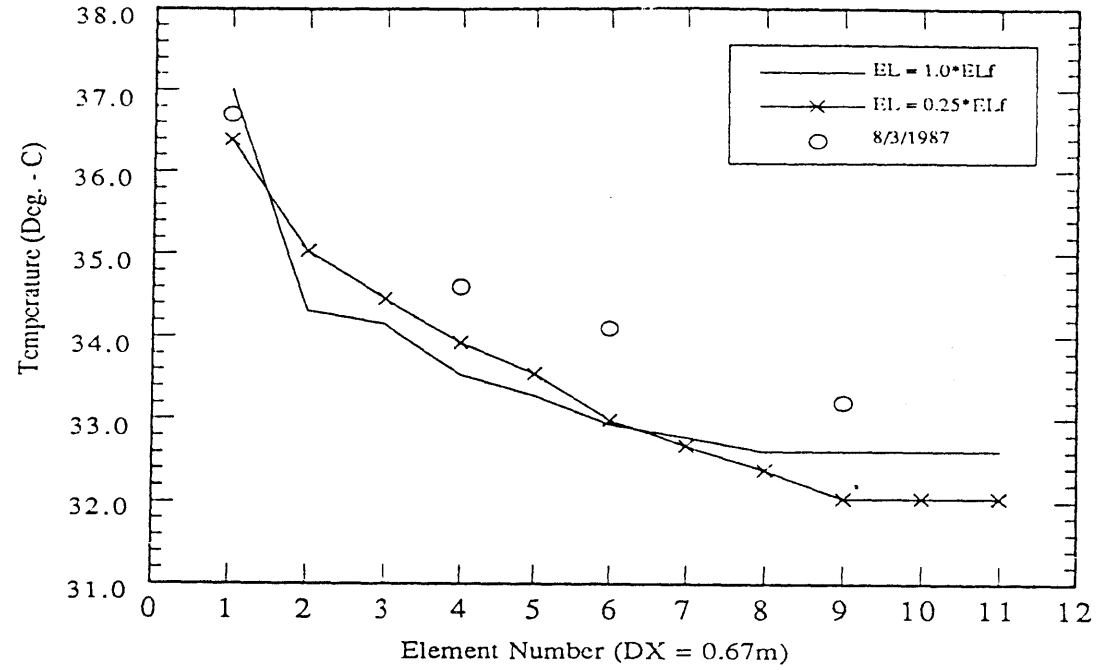

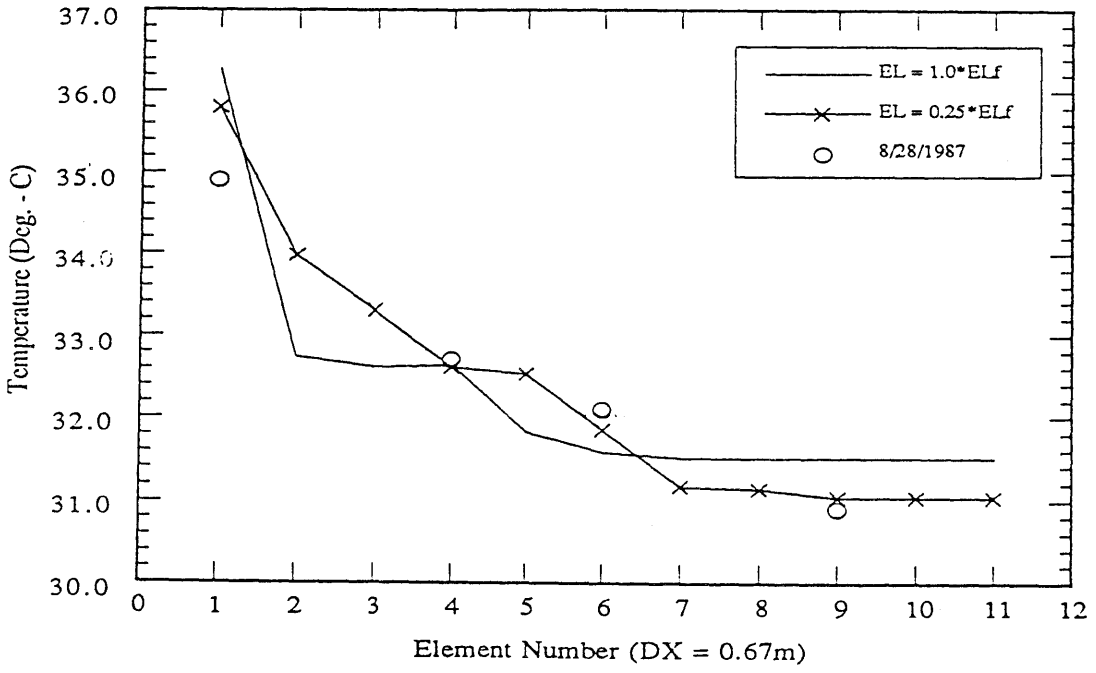

Figure 3-14b Surface temperature variation in Mount Storm Lake as a function of longitudinal dispersion (8/3/87 and 8/28/87)

dilution coefficient as high as 4.6 was estimated (see Appendix A). If the dilution were in fact increased, it would reduce the horizontal temperature gradient at the surface, reduce somewhat the surface cooling, and thus bring the simulation into closer agreement with the observation. Also it would be closer to the theoretical estimate. The results of the sensitivity analysis are summarized in Table 3.5. It shows that for higher values of D_v ($\approx$ 2.5) the error across the epilimnion does not vary much between MSL-1 and MSL-5. However, the temperatures are under predicted by over 1.0° C. However, at $D_v = 2.15$, the best value obtained for the dilution, the mean error at MSL-1 is 0.0° C. The error across the epilimnion however is reduced from 0.94° C to 0.46° C. Therefore, $D_v = 2.15$ was used for all further calculations.

3.3.4 Analysis of the Time Series Errors

3.3.4.1 Analysis of Periodicity in the Errors

The resulting time series of errors at the three diagnostic locations (MSL-1 (surface and bottom) and MSL-5 (surface)) with the corrections described above for ϕ_s, E_L, and D_v are plotted in Figure 3.15 and show what initially appears to be a periodic error. It may be reasonably expected that such an error would have a period of about one year. To explore this periodicity, we use Ho's (1984) method of time series analysis and assume that both the measurements and prediction are periodic functions, P(t) and M(t) respectively (Figure 3.15 shows that this is a reasonable assumption). Then the error,

$$E(t) = P(t) - M(t) \tag{3.11}$$

where

Table 3.5

Sensitivity of Prediction Errors to D_v

D_v	Mean surface error at MSL-1	Std dev	Surface delta error $Error_{MSL-1} - Error_{MSL-5}$
	(°C)		(°C)
3.7	-2.39	1.18	-0.73
3.0	-1.88	1.17	-0.36
2.5	-1.35	1.18	0.01
2.25	-1.03	1.21	0.23
2.2	-0.95	1.22	0.29
2.15	0.0	1.36	0.46
2.125	0.02	1.36	0.48
2.0	0.2	1.4	0.65
1.9	0.35	1.42	0.79

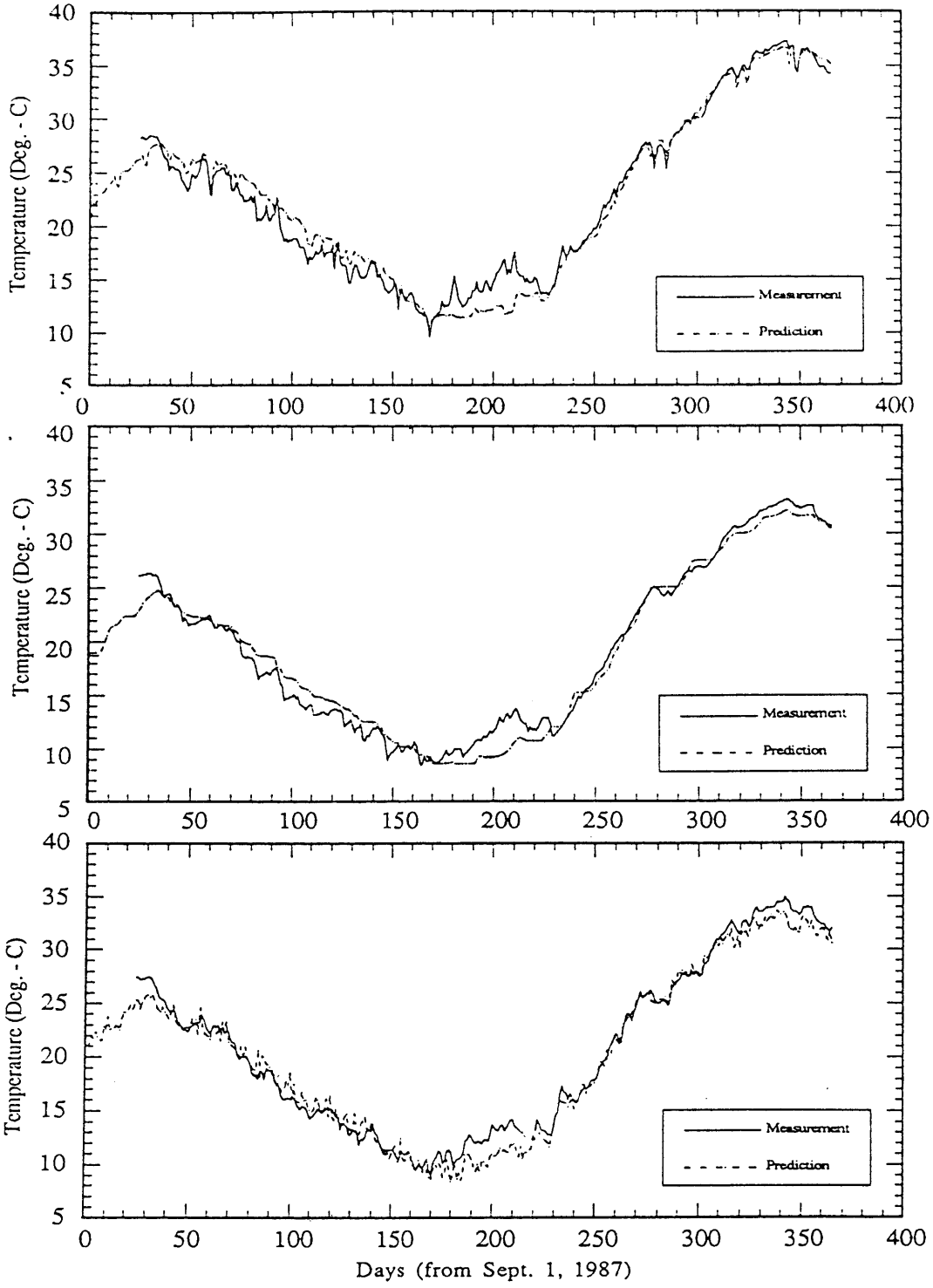

Figure 3-15 Time series of measurements predictions :: Top : Max. surf. temp. (MSL-1)
Middle : Bot. temp. (MSL -1) Bottom : Min. surf. temp. (MSL-5)

$$P(t) = P^*\sin(\omega t + \phi_p) + \epsilon_p(t) \tag{3.12}$$

$$M(t) = M^*\sin(\omega t + \phi_m) + \epsilon_m(t) \tag{3.13}$$

and P^*, M^* are the amplitudes of the prediction and measurement, ϕ_p, ϕ_m are the phases, and ϵ_p, ϵ_m are the random errors of both processes.

For a time series D(t), evaluated at n discrete time intervals over a period T, we can write

$$D(t) = C(t) + \epsilon(t) \tag{3.14}$$

where C(t) is the underlying periodic time series and $\epsilon(t)$ is a random process.

If $C(t) = C^*\sin(\omega t + \phi) = A\sin\omega t + B\cos\omega t$ then the Fourier components of

$$D(t) = A\sin(\omega t) + B\cos(\omega t) + \epsilon(t) \tag{3.15}$$

by direct integration are

$$A(\omega) = \frac{2}{n}\sum_{1}^{n} D(t)\,\sin(\omega t) \tag{3.16}$$

$$B(\omega) = \frac{2}{n}\sum_{1}^{n} D(t)\,\cos(\omega t) \tag{3.17}$$

and therefore the amplitude is

$$C^* = (A^2 + B^2)^{\frac{1}{2}} \tag{3.18}$$

and the phase

$$\phi = \tan^{-1}(B/A) \tag{3.19}$$

The preceding analysis is used to evaluate the time series of predictions, observations, differences between predictions and observations, and station generation to examine any periodic correlations among them. The results obtained using a period $T = 2\pi/\omega$ equal to one year are summarized in Table 3.6.

The last column shows the percentage of the variance that is captured by the periodic function and is estimated as 50% × (amp)²/variance. This column in particular confirms that the predictions and measurements are periodic functions that are in phase. The periodic functions have a phase of about 130 days. Noting that our time series start on September 25, this means that the temperatures peak at about -40 days (i.e., mid-August) and reach their minimum at about 140 days (i.e., mid-February) from the start of the simulation (see Figure 3.15). It also shows that the differences between predicition and measurement and the station generation are not strongly periodic (at least, not with a frequency of one year).

3.3.4.2 Correlation of Residual Error with Mount Storm Station Generation

Figures 3.12a and 3.12b showed that the time series of the Mt. Storm Station power generation is strongly correlated with the time series of the residual errors. The model overpredicts when the station generation is high and underpredicts when the generation is low. The analysis of the previous section already showed that these series do not have a strong annual cycle. Therefore other potential causes for the correlation were examined.

One hypothesis for the cause of this correlation is that the actual flow rate at the station is a function of the station generation. We have assumed that the condenser

Table 3.6

Analysis of Amplitude and Phase of Time Series

Data	Mean	Std dev	Amplitude of periodic function	Phase (days)	Percentage of variance captured by periodic function
Station generation in MWH	27149	7206	5567	76.8	29.8
Observations (in °C)					
MSL-1 (surface)	23.21	7.94	10.95	132.1	95.1
MSL-1 (bottom)	19.81	7.87	10.97	132.3	97.1
MSL-5 (surface)	21.17	7.94	11.07	133.9	97.2
Predictions (in °C)					
MSL-1 (surface)	23.28	8.23	11.32	126.2	94.7
MSL-1 (bottom)	19.71	7.85	10.91	128.3	96.6
MSL-5 (surface)	20.73	7.92	11.00	132.0	96.4
Differences (in °C)					
MSL-1 (surface)	0.07	1.34	1.18	56.4	38.6
MSL-1 (bottom)	-0.10	1.15	0.77	34.2	22.6
MSL-5 (surface)	-0.44	0.98	0.36	30.4	6.8

flow rate was a constant and that all the variation in station generation could be represented by a corresponding change in the condenser temperature rise. If however the condenser flow rate is also varying such that the flow rate is lower during periods of low station generation (this could correspond to using two pumps rather than three) then the condenser temperature rise would be higher during periods of low generation and lower during periods of high generation than we simulated. The result of testing this hypothesis is summarized in Table 3.7. The first column represents what fraction (f_{qv}) of the variation in the station generation is correlated to the condenser flow rate. For example, when f_{qv} is 2/3, then the flow rate Q(t) is estimated as

$$Q(t) = \left[1 + \frac{2}{3}\left[\frac{P(t) - P_{ave}}{P_{ave}}\right]\right] Q_{ave} \tag{3.20}$$

and the corresponding condenser temperature rise (keeping the heat input the same) is

$$\Delta T(t) = \frac{Q_{ave}\Delta T_{ave}}{Q(t)} \tag{3.21}$$

where Q_{ave} is the flow rate used in the model (which was estimated by Virginia Power), ΔT_{ave} is the corresponding temperature rise, which is based on Q_{ave} and the average power P_{ave} generated during the simulation year, and P(t) is the daily power generation. If in fact the hypothesis is true, then the variance of the error should decrease and different degrees of correlation should be observed at the three locations. That is, the model would have a higher correlation at MSL-1 than at MSL-5 where the effects of the flow rate variation are less direct. From Table 3.7, the biggest decrease in the standard deviation (at all stations) occurs for $f_{qv} = 1/8$, and, as expected, the decrease is bigger at the two MSL-1 stations. Compared with

Table 3.7

Errors Associated with Variation in Condenser Flow Rate: Q_v ($D_v = 2.15$)

fraction of variation in station generation affecting flow, f_{qv}	Mean error °C MSL-1 (surface)	MSL-1 (bottom)	MSL-5 (surface)	Std dev MSL-1 (surface)	MSL-1 (bottom)	MSL-5 (surface)
1	0.21	-0.06	-0.14	1.75	2.05	1.64
2/3	-0.19	-0.37	-0.53	1.53	1.59	1.23
1/3	-0.52	-0.66	-0.88	1.31	1.19	0.97
1/4	-0.54	-0.68	-0.89	1.26	1.09	0.94
1/8	-0.5	-0.65	-0.89	1.20	1.00	0.93
1/10	-0.39	-0.53	-0.78	1.21	1.01	0.93
1/20	-0.06	-0.20	-0.50	1.34	1.18	1.00
0 (base case)	0.0	-0.15	-0.46	1.36	1.17	1.00

the base case ($f_{qv} = 0$), the standard deviation of the prediction error using $f_{qv} = 1/8$ drops from 1.36° C to 1.20° C at MSL-1 (surface), from 1.17° C to 1.00° C at MSL-1 (bottom), and from 1.00° C to 0.93° C at MSL-5 (surface). These represent changes in variance of 22%, 27%, and 14% respectively. (For example, $(1.36^2 - 1.20^2) \times 100\%/1.36^2 = 22\%$.) We conclude that variation in flow rate does affect the model's response. However since the actual variation is unknown and the sensitivity test did not result in a large reduction of variance, the model was not modified to account explicitly for any variation in flow.

Instead, an empirical approach was used to identify any non-random relationship between the model-measurement errors and the station generation. The correlation function between the station generation and each of the errors is summarized in Figure 3.16a as a function of the lag interval. It confirms that there is indeed a correlation and that the correlation peaks at about 18 days. That is, the best correlation is between prediction error and station generation 18 days earlier. Eighteen days is approximately equal to the thermal time constant of the lake (see Chapter 4), which implies that the lag may be due to the thermal inertia of the lake.

The slow decrease of the correlation function in Figure 3.16a shows that there is some trend that has a period of about 240 days (the distance between the two peaks). It is clear that this is just the pattern of station generation that year since there is no known physical trend with that period that would explain this. Figure 3-16b shows a scatter plot of the errors at MSL-1 (surface) with the station generation. Although there is considerable scatter, a simple linear regression model would account for about 25% of the error (the coefficient of determination is approximately $0.5^2 = 0.25$). The least squares regression between the error and the station generation may be written as

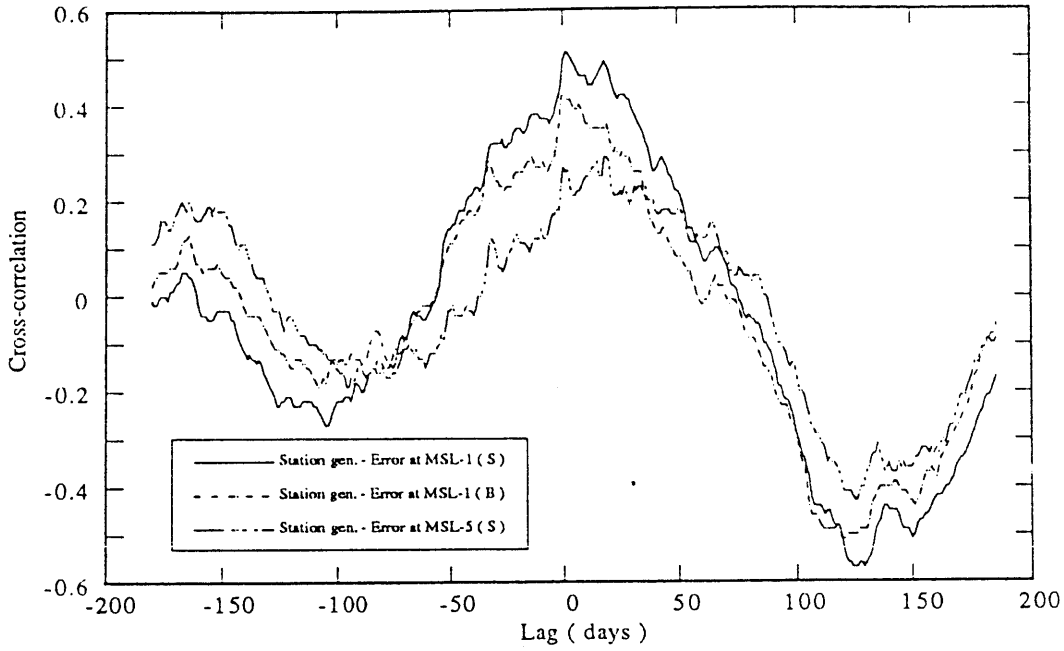

Figure 3-16a Correlation between station generation and model errors

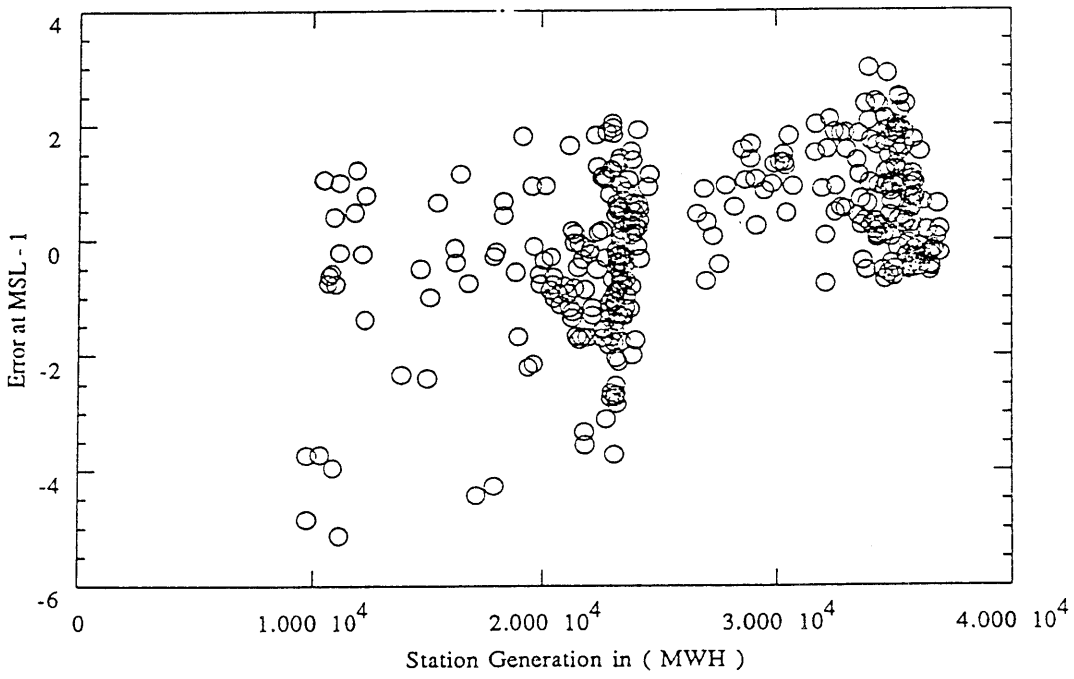

Figure 3-16b Error at MSL-1 (surf) vs. station generation

$$\text{error} = \text{mean error} + \beta_1(\text{power gen.} - \text{mean power generated}) \qquad (3\text{-}22)$$

where β_1 is the slope. A model utility test rejects the null hypothesis H_0: $\beta_1 = 0$ (which if true would mean that the errors are independent of the station generation) at all levels of significance. Therefore the linear model may be used to correct the model output. Figure 3-17 shows the time series of the errors at MSL-1 (surface) for the same simulation year corrected for the station generation. This series has a mean of zero, as would be expected. The variance of the errors is also reduced by about 23% from 1.36^2 to 1.19^2. At the other locations, the reduction in variance is less because the coefficient of determination for the linear regression is lower. This fact is significant in that it confirms the earlier hypothesis that the correlation between the station generation and the errors is expected to be higher at MSL-1 (surface) than at the other locations.

In conclusion, significant correlation between prediction errors and station generation is apparent. While this correlation could not be explained physically, it is likely related to the way station heat rejection is computed from station generation data. Correcting for the correlation, using linear regression between model errors and station generation, reduces model variance by up to 23%.

3.4 Verification of the 1-D Model (Second-Year Simulation, Sept. 1987 - Aug. 1988)

Verification consisted of comparing model predictions, with the calibrated model, against observation for a second year. (No change was made in model parameters for the second-year simulation.) The results are summarized in Figures 3.18-3.25 which show the temperature profiles and Figure 3.26 which shows the time series of model-observation differences at the three locations MSL-1 (surface),

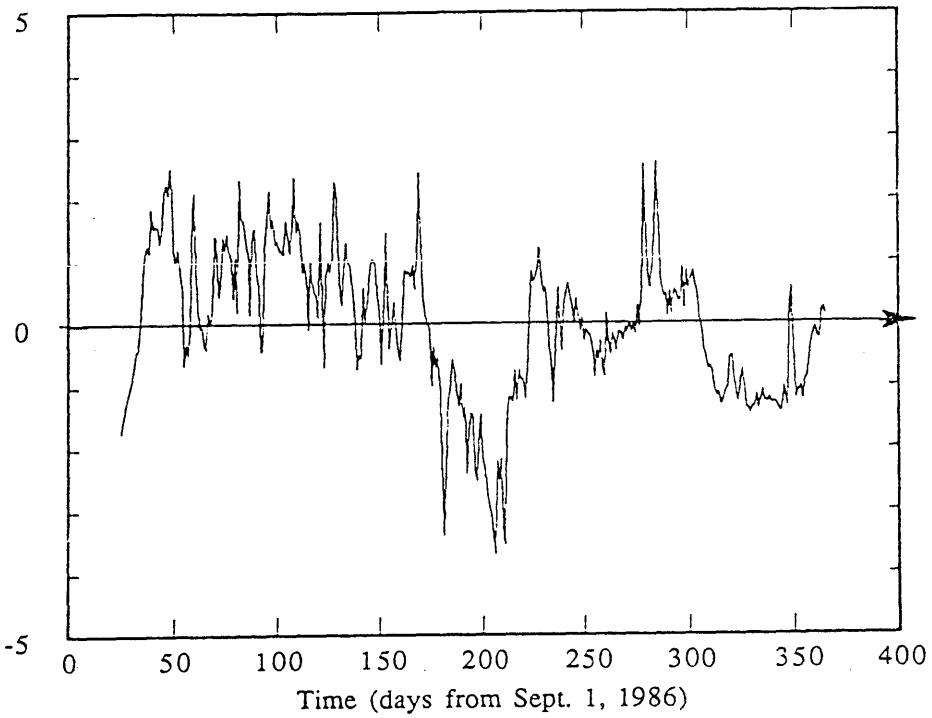

Figure 3-17 Corrected time series of errors at MSL-1 (first simulation year)

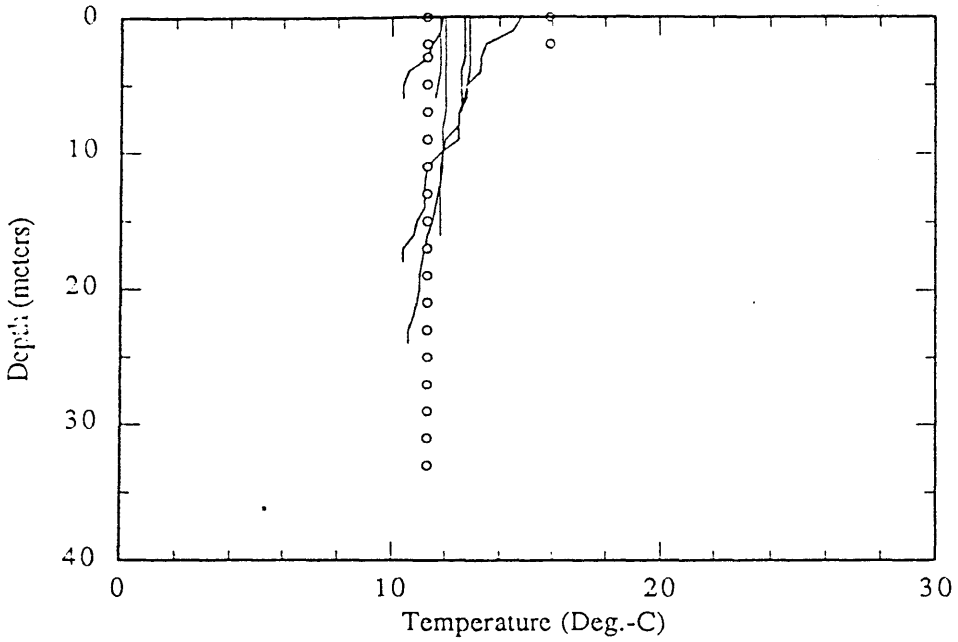

Figure 3-18 Measured and Predicted Temperature Profiles for January 15, 1988

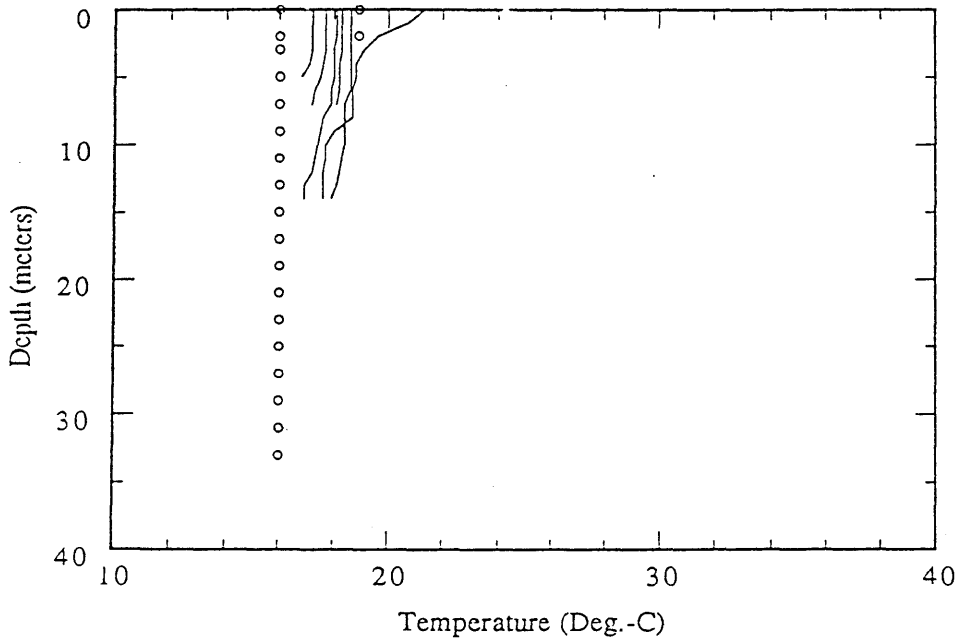

Figure 3-19 Measured and Predicted Temperature Profiles for April 20, 1988

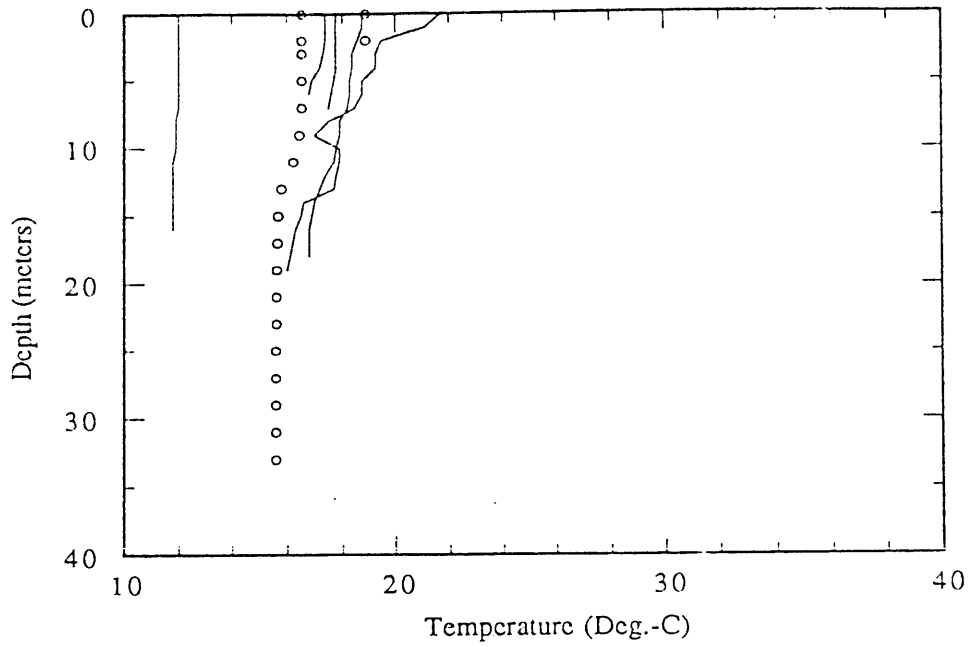

Figure 3-20 Measured and Predicted Temperature Profiles for May 4, 1988

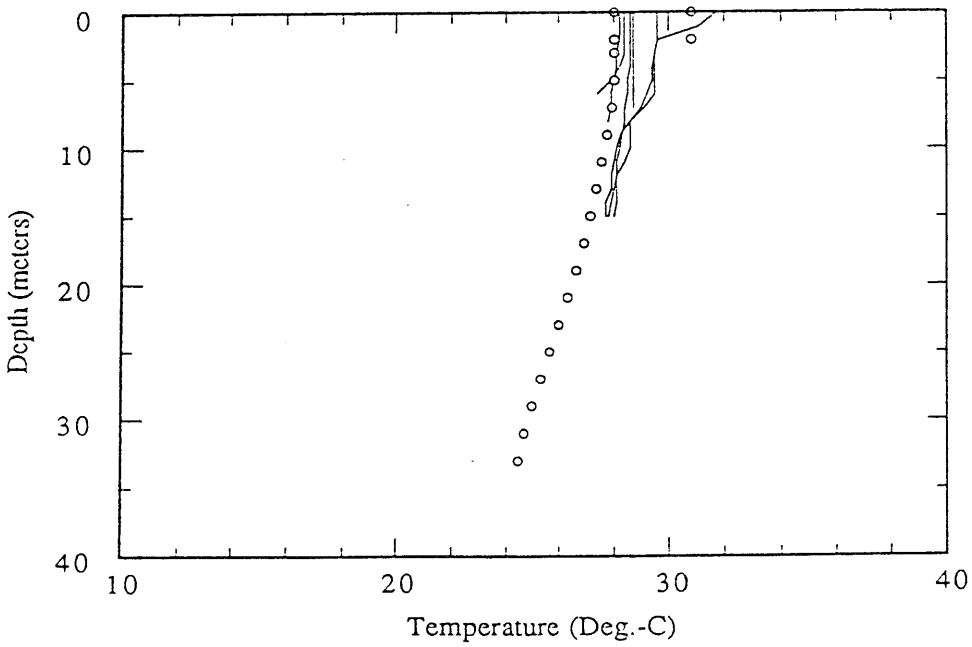

Figure 3-21 Measured and Predicted Temperature Profiles for June 21, 1988

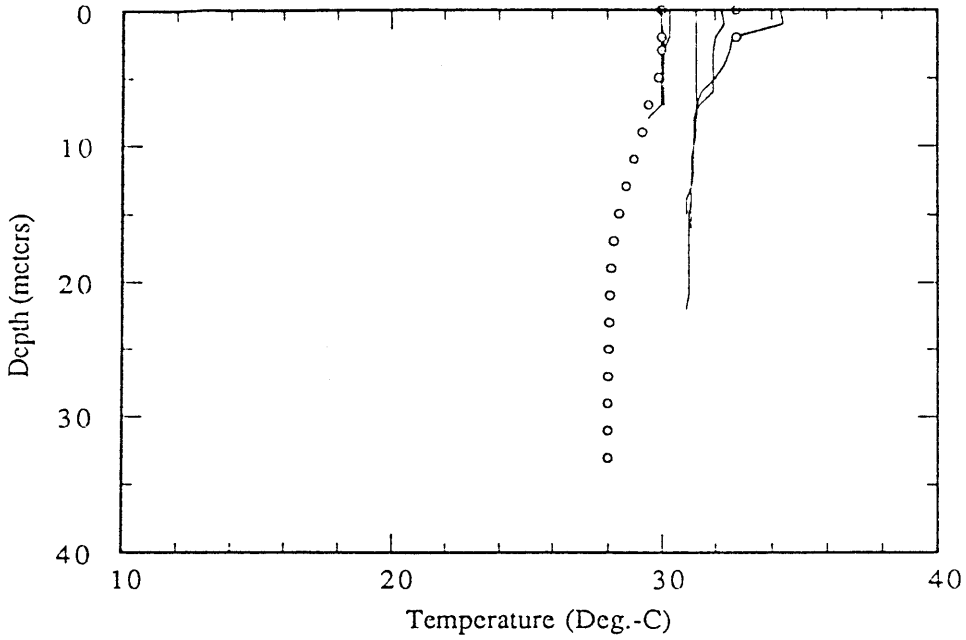

Figure 3-22 Measured and Predicted Temperature Profiles for July 7, 1988

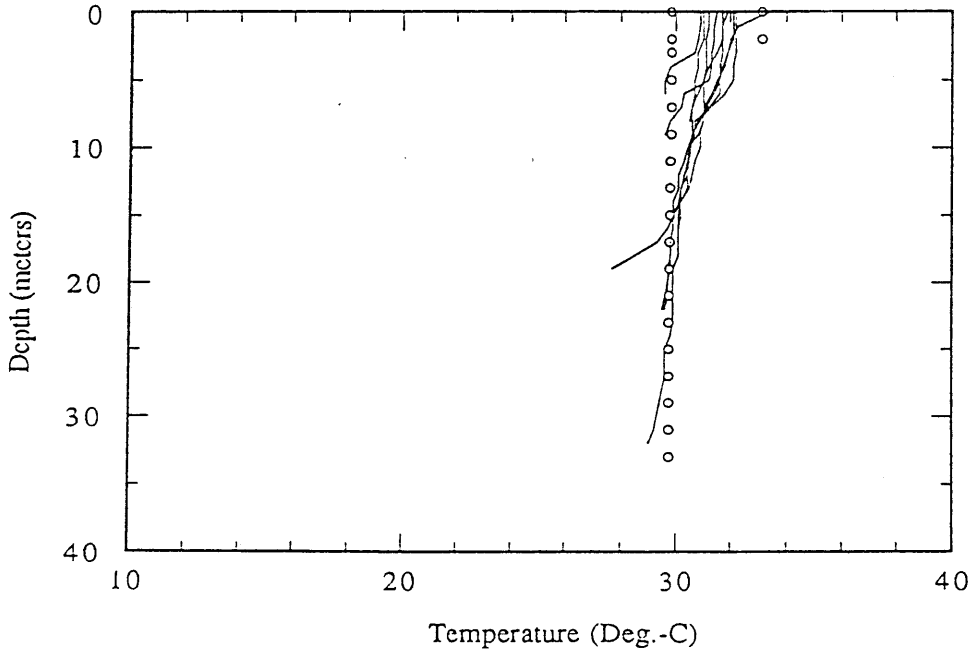

Figure 3-23 Measured and Predicted Temperature Profiles for July 28,1988

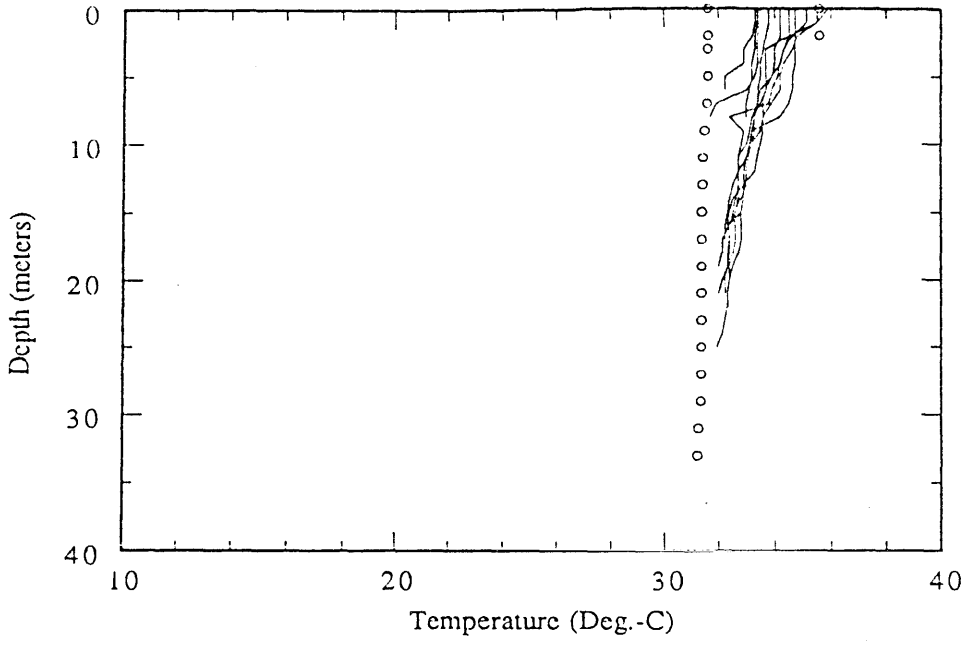

Figure 3-24 Measured and Predicted Temperature Profiles for August 9, 1988

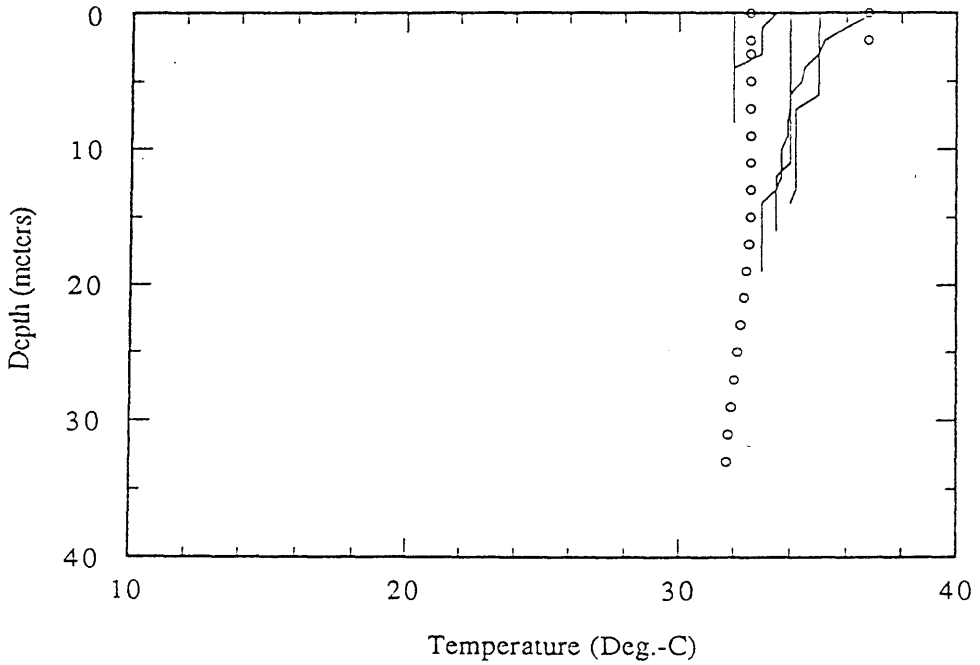

Figure 3-25 Measured and Predicted Temperature Profiles for August 16, 1988

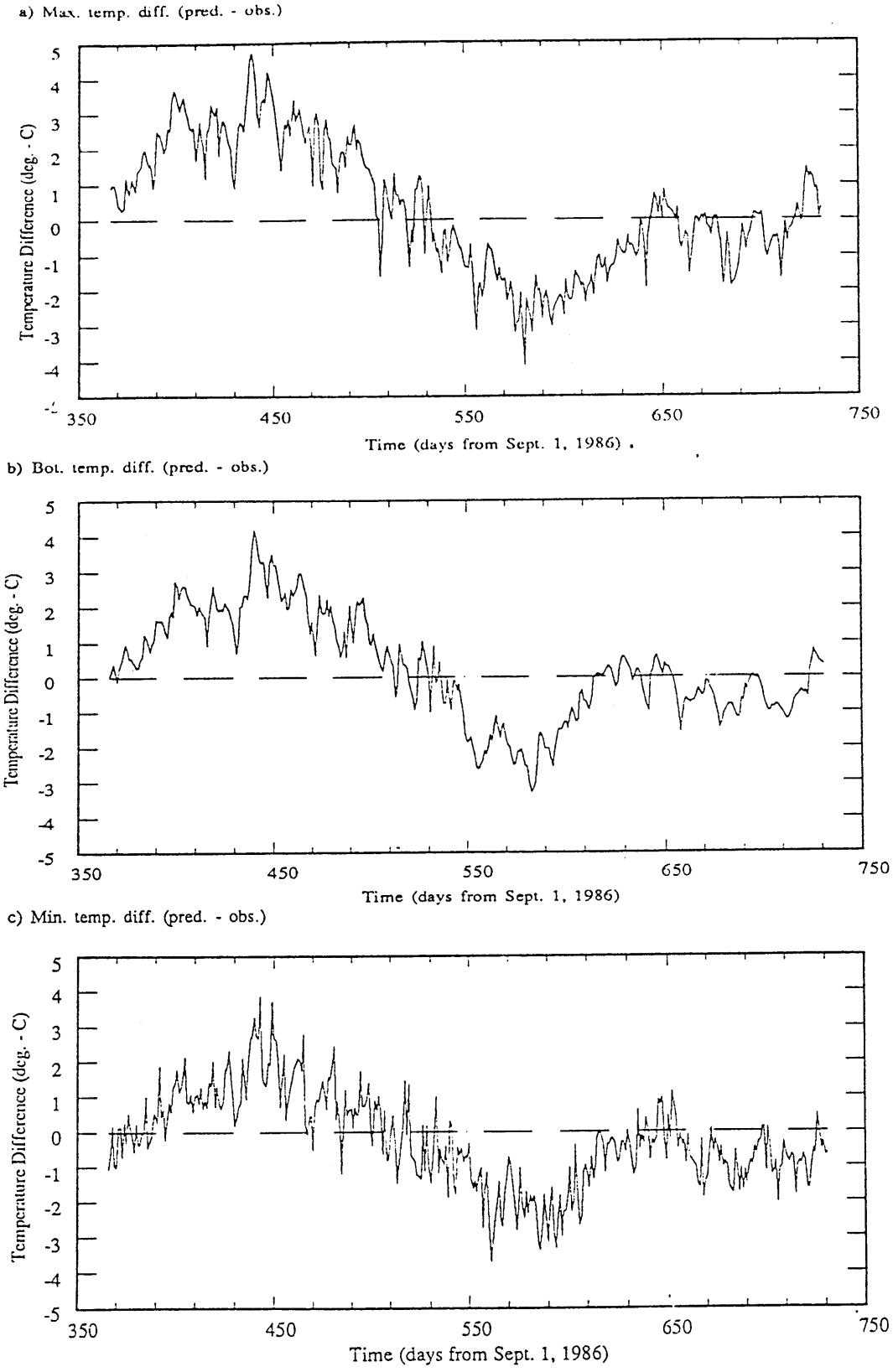

Figure 3-26 Time series of temperature differences second year (Sept. 1987 - Aug. 1988)

MSL-1 (bottom), and MSL-5 (surface). Most of the profiles show good qualitative agreement with the observations. The error statistics for the new predictions are summarized in Table 3.8.

The annual average error at the three stations ranges from 0.35° C to -0.24° C with a mean of 0.11° C and a standard deviation of about 1.5° C. After applying the linear regression correction (based on the previous year's data) to the model output, the mean model error is reduced to about 0.06° C and the variance at MSL-1 is also reduced by about 25%. (Note that the application of the linear regression model is approximate since the station generation is not a stationary process. The mean power generation varies from year to year.)

We conclude that the 1-D model is verified by the second year of data and that MITEMP may be used reliably to assess the thermal impacts of power generation on Mount Storm Lake for any year with an "accuracy" of about ±1.5° C. This accuracy is based on the computed RMS model error (without using the linear correlation) defined by

$$\text{RMS error} = [(\text{mean error})^2 + (\text{std dev})^2]^{\frac{1}{2}} \tag{3.23}$$

Using data from the verification year (Table 8), this error is 1.84° C at MSL-1 (surface), 1.53° C at MSL-1 (bottom), and 1.35° C at MSL-5 (surface) with an average of 1.57° C.

Table 3.8

Error Statistics of Time Series for Second-Year Validation (Sept. 1987 - Aug. 1988)

	Mean			Std. Dev.		
	Pred	Obs	Diff	Pred	Obs	Diff
MSL-1 (surface)	24.29	23.94	0.35	7.61	7.42	1.81
MSL-1 (bottom)	20.23	20.00	0.23	7.55	7.52	1.51
MSL-5 (surface)	21.40	21.64	-0.24	7.46	7.45	1.33
Average			0.113			

4 DEVELOPMENT OF 0-D MODEL

As mentioned in Chapter 1, the purpose of this study is two-fold. The first was to modify and test the 1-D model (MITEMP) described in the previous chapters. The other purpose is to compare other models of varying complexity with the 1-D model. This chapter discusses a 0-D model that was developed in response to a water supply study performed for Virginia Power.

Several scenarios being considered by Virginia Power involve current and future electricity production that would increase water consumption at Mt. Storm Lake. Increased consumption, in turn, could lead to decreasing water levels (increased drawdown) and increased water temperatures due to the reduced lake surface area. In order to study these possibilities, a study was made to examine the effect on drawdown and temperature rise of each scenario (see Adams and Adelaja, 1989). Because a large number of scenarios was involved (resulting in over 1000 simulations), that study used a simple 0-D screening model described below based on monthly averaged data. The use of monthly averages was dictated by the data availability, but as will be shown later appeared rational based on both the computed thermal time constant and a comparison with the 1-D model simulation. The 0-D model was combined with a streamflow generation model to determine a water balance and hence the monthly drawdown associated with each scenario. The model was very efficient requiring only a few minutes of CPU time on the microVax to simulate over a thousand years' worth of data.

4.1 Temperature Predictions with 0-D Models

For a 0-D model, the fully mixed assumption means that the water temperature in the lake is constant everywhere and under steady-state conditions is equal to the

equilibrium lake temperature (which for present purposes includes the thermal input from the power plant). The MITEMP model described in Chapters 2 and 3 used daily averaged meteorological data. The temperature predictions of the steady-state model may be compared with the results of the transient MITEMP model using the first year of simulation data by using 30-day averages of the meteorological data to evaluate the equilibrium temperature for the steady state model. Note that the use of averaged data results in a damping of transient fluctuations similar to the thermal damping provided for in a transient model. The well-mixed assumption results in a temperature that should fall on average between the spatial maximum and minimum prediction from the 1-D model.

The former point is explored by examining the *time-varying* governing equation for a well-mixed cooling lake

$$\frac{\partial}{\partial t}(\rho c \forall T) = -\phi_n A \tag{4.1}$$

where the components of the net heat flux ϕ_n through the water surface have been described in Section 2.1.3. Several of these components are nonlinear functions of the water surface temperature but may be linearized through the concept of an equilibrium temperature and the surface heat exchange coefficient K, using the approach first developed by Edinger and Geyer (1965). Eq. (4.1) then becomes

$$\frac{d}{dt}(\rho c \forall T) = -K(T - T_E)A \tag{4.2}$$

The solution to this equation for $\forall$ and A constant and step changes in T_E over a time interval Δt is given by Adams and Koussis (1980) as

$$T(t) = \left[1 - e^{\frac{-K\Delta t}{\rho c H}}\right] \sum_{n=0}^{\infty} T_E(t - n\Delta t) e^{\frac{-K\Delta t}{\rho c H}} \qquad (4.3)$$

where H is the average lake depth ∀/A. Eq. (4.3) shows that the *transient response* of a spatially well-mixed lake may be viewed as a time series of *steady state responses* to an input series of equilibrium temperatures that have passed through an exponential filter (Adams and Koussis, 1980). The exponential filter provides damping governed by the thermal time constant ρcH/K. For Mount Storm Lake, H ≃ 40 feet and based on a typical value of K = 150 BTU/ft^2-°F-d, ρcH/K ≃ 17 days. With this interpretation, Eq. (4.3) can be compared with a steady-state model that uses straight averaged data (e.g., monthly averages). Figure 4.1 shows the unfiltered equilibrium temperatures compared with the 1-D model (MITEMP) while results from Eq. (4.3) using the exponential filter are shown in Figure 4.2.

It should be apparent that the *steady-state* model used for the water availability study is similar to the above *transient* model except that it uses an averaging filter with a constant interval of 30 days rather than an exponential filter with a time constant of 15-20 days. The effect of using different averaging intervals is shown in Figures 4.3-4.6 where it can be seen that greater damping is achieved as the averaging interval increases. These results may be compared with the result from the 1-D model. Since the well-mixed assumption is expected to result in temperature predictions that are somewhere between the maximum and minimum temperatures predicted by the 1-D model, the results are compared with the observations at MSL-5 (surface). The results are summarized in Table 4.1. The table shows that the models are all fairly accurate on average (within ±0.35° C) in simulating the lake temperature at MSL-5, though the quasi-steady model is the most accurate. This is expected since it is a transient model. However it is clear

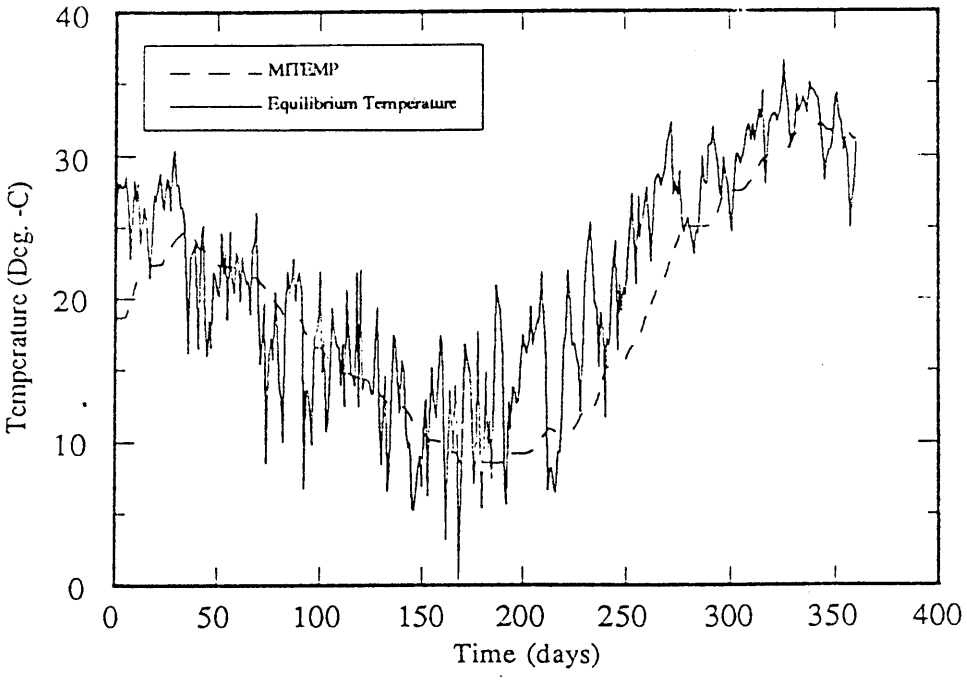

Figure 4-1 Comparison of MITEMP predictions with unfiltered equilibrium temperature

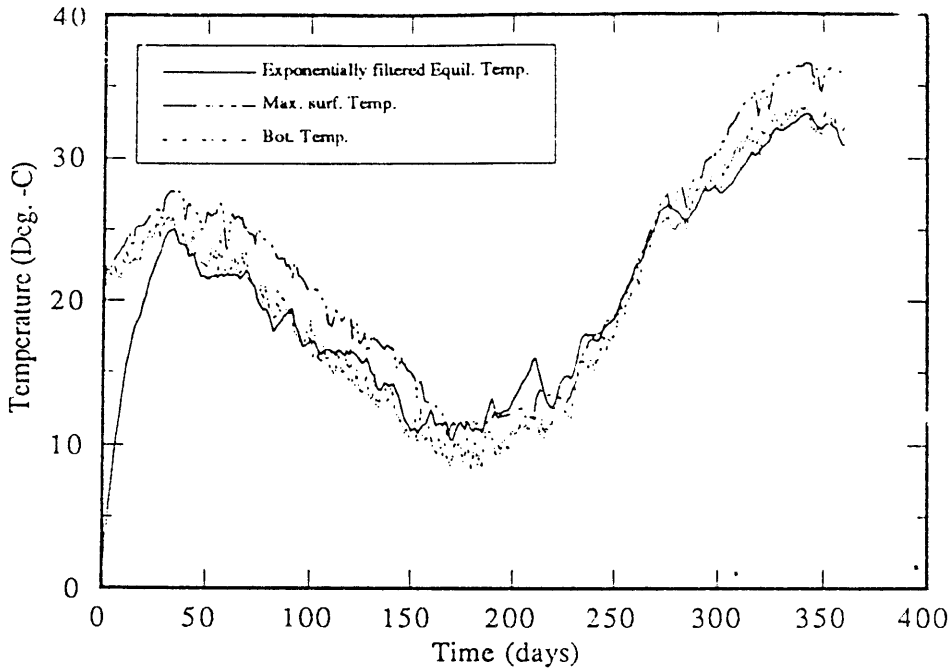

Figure 4-2 Comparison of MITEMP predictions with quasi-steady model

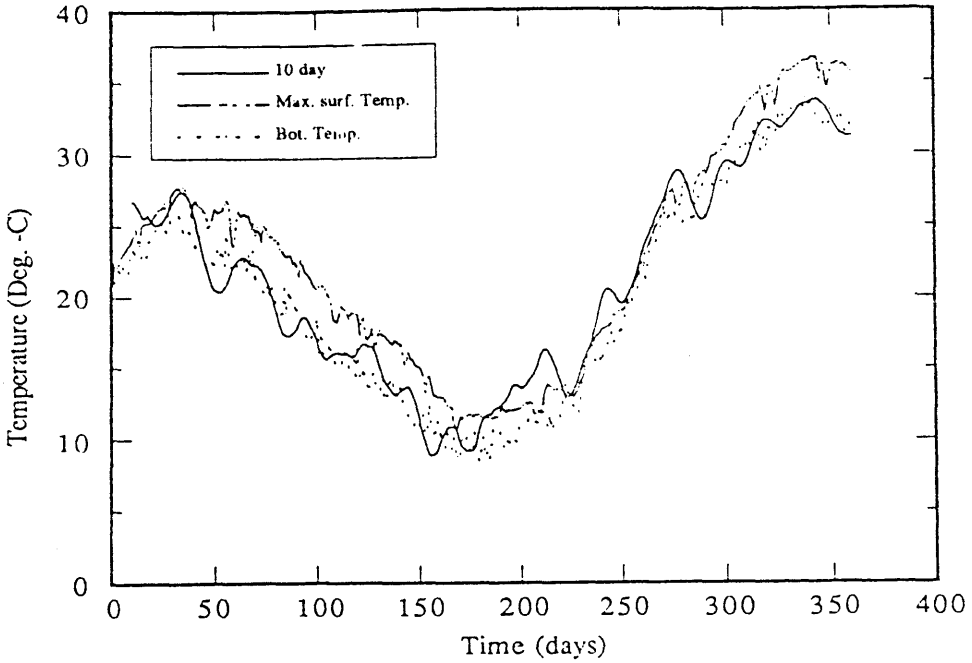

Figure 4-3 Comparison of MITEMP predictions with steady-state model using 10d-averaged meteorological data

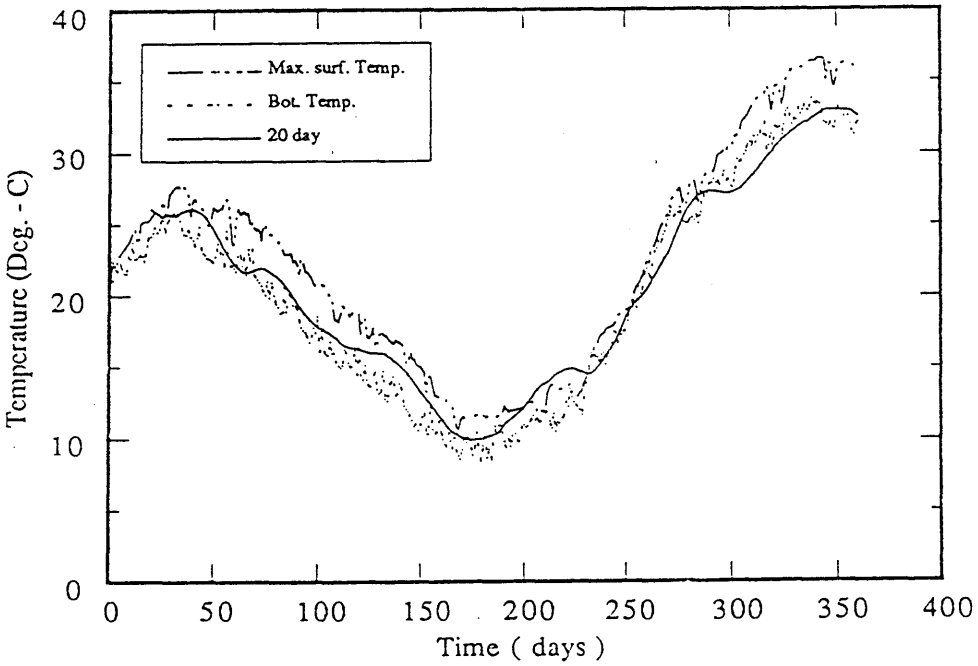

Figure 4-4 Comparison of MITEMP predictions with steady-state model using 20d-averaged meteorological data

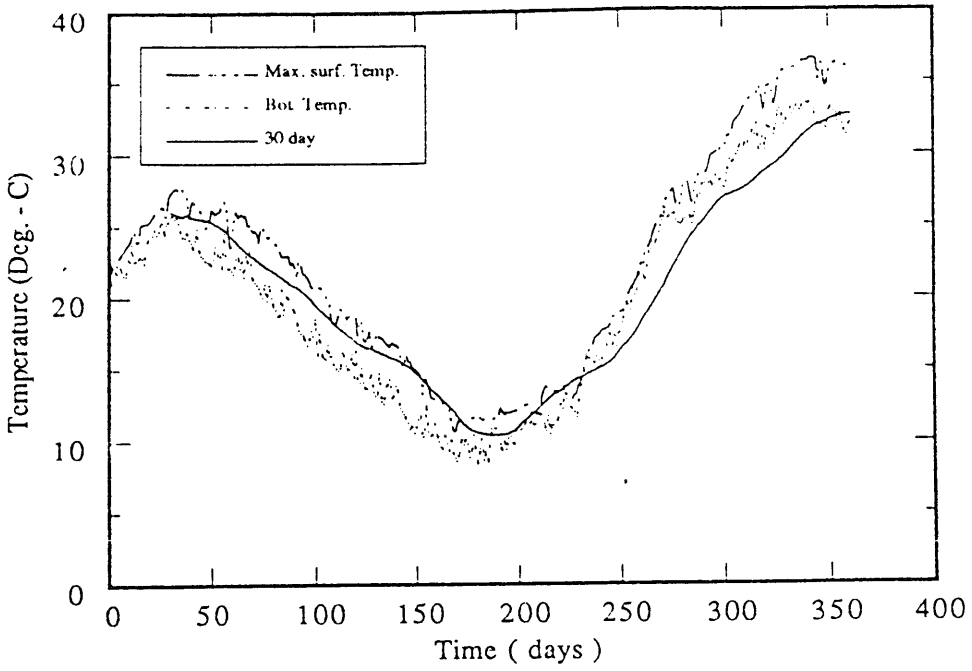

Figure 4-5 Comparison of MITEMP predictions with steady-state model using 30d-averaged meteorological data

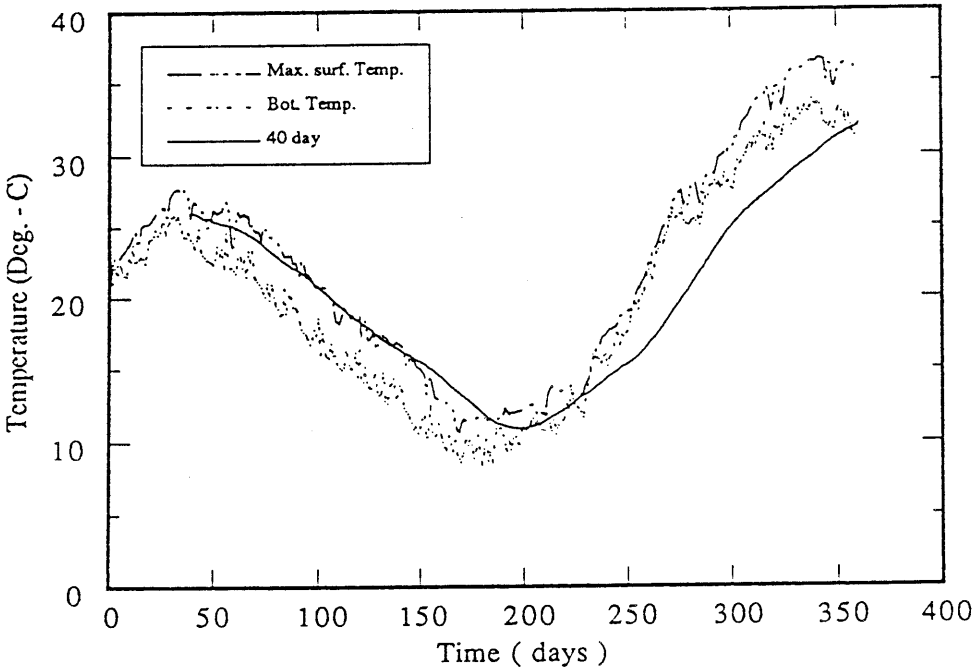

Figure 4-6 Comparison of MITEMP predictions with steady-state model using 40d-averaged meteorological data

Table 4.1

Error Statistics of Steady State Model

Averaging interval (days)	Mean error (pred - obs*) (°C)	St dev	Max pred temp (°C)	Min pred temp (°C)	Max temp diff (°C)
10	-0.34	1.51	28	8	20
20	0.14	1.61	27	10	17
30	-0.05	2.49	26	11	15
40	-0.23	3.57	26	12	14
quasi steady model	0.08	1.23	25	11	14

*obs at MSL-5 (surface)

that the 0-D model would not compute the time variability at MSL-1 (near the discharge) so accurately. The last three columns show the maximum and minimum temperatures predicted by each model during the simulation period of a year as well as the difference between the two. It appears from these results and from Figures 4.3-4.6 that a 20-day average might have been closer on average than the 30-day average that was used. With the shorter interval of 10 days, the response is much faster than the lake, while with larger intervals like 40 days, the model is damped. However the 30-day average is also reasonable, particularly during the summer months. This is in agreement with the conclusion arrived at by Adams and Koussis (1980) that acceptable results may be obtained using a steady-state model with averaged meteorology if an averaging interval of between one and two times the time constant is used.

In conclusion, the steady well-mixed model developed for studying the water availability may be used to estimate the temperature in the lake fairly accurately. For all averaged intervals, the absolute mean error (prediction-observation at MSL-5 (surface)) is less than 0.35° C while the standard deviation varies from 1.5° C for the 10-day averaging interval to 3.6° C for the 40-day interval. The 30-day average has a mean error of -0.05° C and standard deviation of 2.5° C so the RMS error (accuracy) for the 0-D model with monthly average data is about 2.5° C ($2.5^2 + 0.5^2 \simeq 2.5^2$). Meanwhile, the quasi-steady model has a mean error of less than 0.1° C and a standard deviation of about 1.2° C, again based on data at MSL-5 (surface). This compares with a calibrated accuracy for MITEMP at MSL-5 of about 1.0° C for the first simulation year (see Table 3.7) and about 1.3° C for the second year (see table 3.8). Considering the substantial approximation, the 0-D models are considered useful for purposes of initial screening.

5 THE 2-D MODEL NARES

The preliminary analysis showed that Mount Storm Lake may be classified as a vertically stratified pond with horizontal temperature structure only in the epilimnion. Hence the vertically stratified submodel in MITEMP was used The purpose of this chapter is to determine whether a fully 2-D model (with horizontal temperature variability throughout the pond) is capable of capturing the actual temperature variation in the lake more accurately than the essentially one-dimensional model.

NARES is a two-dimensional, laterally averaged transient, hydro-thermal, finite difference model originally developed by Wang and Kravitz (1980) for simulation of estuarine circulation, and later adapted by Huang et al. (1988) to simulate the hydro-thermal processes in a water supply reservoir, the Wanaque. The original model employs a semi-implicit solution scheme, whereby the model generates time series of water surface elevation, horizontal and vertical velocities, and salinity at discrete grid points in a vertical plane (Huang et al., 1988). The variations of variables and parameters in the transverse direction are assumed to be small which is an appropriate assumption in a deep and relatively narrow reservoir with moderate vertical stratification such as Mount Storm Lake. The Wanaque is geometrically similar to Mt. Storm Lake; the maximum and averaged depths are about 90 feet and 40 feet respectively for both lakes while the lengths of both reservoirs are about ten times the average widths. Therefore, the model appears appropriate for use in simulating Mt. Storm Lake.

5.1 Description of the Two-Dimensional Model

5.1.1 Model Formulation

The governing equations for two-dimensional laterally averaged flow for the modified model are the following (Wang and Kravitz, 1980; Huang et al., 1988)

Equation of continuity:

$$\frac{\partial}{\partial x}(uB) + \frac{\partial}{\partial x}(wB) = 0 \tag{5.1}$$

$$\frac{\partial}{\partial t}(B_0\eta) + \frac{\partial}{\partial x}\int_{-H}^{\eta}(uB)dz = 0 \tag{5.2}$$

Momentum equation:

$$\frac{\partial}{\partial t}(uB) + \frac{\partial}{\partial x}(uuB) + \frac{\partial}{\partial z}(uwB) - \frac{\partial}{\partial x}\left[BN_x\frac{\partial u}{\partial x}\right] - \frac{\partial}{\partial z}\left[BN_z\frac{\partial u}{\partial z}\right] + \kappa u|u|\left|\frac{\partial B}{\partial z}\right| + gB\frac{\partial \eta}{\partial x} + \frac{gB_0}{\rho_0}\frac{\partial}{\partial x}\int_z^0 \rho dz' = 0 \tag{5.3}$$

Conservation of thermal energy:

$$\frac{\partial}{\partial t}(TB) + \frac{\partial}{\partial x}(TuB) + \frac{\partial}{\partial z}(TwB) - \frac{\partial}{\partial x}\left[BK_x\frac{\partial T}{\partial x}\right] - \frac{\partial}{\partial z}\left[BK_z\frac{\partial T}{\partial z}\right] - \frac{1}{\rho cB}\frac{\partial}{\partial z}(\phi_{sz}B) = 0 \tag{5.4}$$

Equation of state:

$$\rho = 1.0 - 1.965 \times 10^{-6}\left[\frac{(T+289)(T-4)^2}{(T+68.1)}\right] \tag{5.5}$$

In the above, x and z are the longitudinal and vertical coordinates, u and w are the corresponding velocity components; η is the surface elevation; H the mean water depth; B the width of the estuary; T is the water temperature in degrees Celsius;

K_x, N_x are the longitudinal diffusivity and viscosity respectively; K_z, N_z the vertical diffusivity and viscosity respectively; and κ the boundary friction coefficient.

The boundary conditions are:

Prescribed momentum flux at the boundaries:

$$N_z \frac{\partial u}{\partial z} = \text{wind stress} \quad \text{at} \quad z = \eta \tag{5.6}$$

$$N_z \frac{\partial u}{\partial z} = \kappa u|u| \quad \text{at} \quad z = -H \tag{5.7}$$

Heat flux at the bottom boundary

$$K_z \frac{\partial T}{\partial z} = 0 \quad \text{at} \quad z = -H \tag{5.8}$$

5.1.2 Wind Mixing in the Two-Dimensional Model

The wind-mixing algorithm in the two-dimensional model is a mixed-layer-type model based on Harvey and Davies' (1976) parameterization of wind-mixing. Neglecting advection, the vertical heat balance in a water column may be written as:

$$\frac{\partial T}{\partial t} = \frac{\partial}{\partial z}\left[S + K_z \frac{\partial T}{\partial z} - (\overline{w'T'})\right] \tag{5.9}$$

where S is the downward solar radiation ($= \phi_{sz}/\rho c$) and $(\overline{w'T'})$ is the upward heat flux due to wind and convective mixing. Assuming that the rate of change of potential energy associated with the entrainment of a stagnant lower layer into the turbulent upper layer is equal to the rate of work done by wind-induced shear stresses, the depth of the mixed layer may be determined for a given wind shear stress using the energy available for mixing. At a quasi-steady state, the kinetic and

potential energy attain equilibrium. The temperature profile in the fully mixed layer is stabilized and isothermal. Under this condition, Eq. (5.9) becomes

$$\frac{\partial}{\partial z}[S - (\overline{w'T'})] = \text{constant at } -h < z < 0 \tag{5.10}$$

where h is the mixed layer depth. Integrating over the assumed mixed layer depth h,

$$(\overline{w'T'}) = (\overline{w'T'})_0 - \frac{z}{h}[(\overline{w'T'})_0 - (\overline{w'T'})_{-h}] + S - S_0 + \frac{z}{h}[S_0 - S_h] \tag{5.11}$$

The total turbulent kinetic energy may be related to the wind stress (Huang et al., 1988) by

$$\int_{-h}^{0} (\overline{w'T'})dz = -\frac{u_*^3}{\alpha g} \tag{5.12}$$

where α is the thermal expansion coefficient of water. Integrating Eq. (5.11) once again and recognizing that $(\overline{w'T'})_{-h} = 0$ at the metalimnion, the mixed depth becomes

$$h = \frac{\frac{2u_*^3}{\alpha g} + 2\int_{-h}^{0} S dz}{S_0 + S_{-h} - (\overline{w'T'})_0} \tag{5.13}$$

The boundary conditions are:

$$(\overline{w'T'})_0 = (\phi_{br} - \phi_{an} + \phi_e + \phi_c)/\rho_0 c \tag{5.14}$$

$$S_0 = \phi_{sn}/\rho_0 c \tag{5.15}$$

$$u_* = V_a\sqrt{C_D \rho_a/\rho_0} \tag{5.16}$$

where C_D is the wind drag coefficient and V_a is the wind speed. (Eqs. (5.14) and (5.15) represent the net heat flux at the water surface.) When there is a net surface cooling, $S_0 - (\overline{w'T'})_0 \leq 0$ and

$$h = u_*/f \tag{5.17}$$

where f is the Coriolis constant. The net heat flux at any depth z in the mixed layer may then be calculated as

$$\phi_{(z)} = \rho_0 c(S - \overline{w'T'}) \tag{5.18}$$

where $S = \phi_{sz}/\rho c$ and ϕ_{sz} is ϕ_z in Eq. (2.5).

5.1.3 Solution Procedure/Methodology

The governing equations (5.1)-(5.2) and specified boundary conditions (5.6)-(5.8), (5.14)-(5.16) are solved numerically by the finite difference method using a staggered grid system. Horizontal velocity and temperature are computed at every other node, and vertical velocity at every alternate node.

The difference equations are formulated so that the advancing of the solutions are leap-frogged in time. The Euler-backward scheme is used every ten time steps to eliminate time splitting errors due to extended use of the leap-frog scheme.

A semi-implicit formulation was used in the momentum and continuity equation to increase computational efficiency. Integrating Eq. (5.3) over the water depth yields

$$\frac{\partial}{\partial t}\int_{-H}^{\eta} Bu\, dz + g\frac{\partial \eta}{\partial x}\int_{-H}^{\eta} B dz = \text{remaining terms} \tag{5.19}$$

For the semi-implicit scheme, the left-hand side of the equation as well as Eq. (5.2) are written in the implicit form, and the right-hand side of the equation was computed explicitly, resulting in a tridiagonal system of equations for η^{n+1} when all the variables at time step n are known. After the elevation is updated, the other variables are solved for explicitly.

The model calculates the water densities using Eq. (5.5) and then updates the eddy viscosities and diffusivities. Next the horizontal velocities are computed by the difference form of Eq. (5.3), and the vertical velocities by Eq. (5.1). Using the wind mixing algorithm described in Section 5.1.2, the wind mixing depths and the heat fluxes are calculated. Finally the water temperatures are calculated using the difference form of Eq. (5.4). The meteorological and inflow/outflow input data for the next time step are read in or interpolated and the state variables are updated by repeating the above procedures.

5.2 Application to Mount Storm Lake

5.2.1 Schematization

The two-dimensional staggered grid system employed by the model for Mount Storm Lake is shown in Figure 5.1. As in the one-dimensional model, the longitudinal dimension is represented by eleven crossections with an interval of

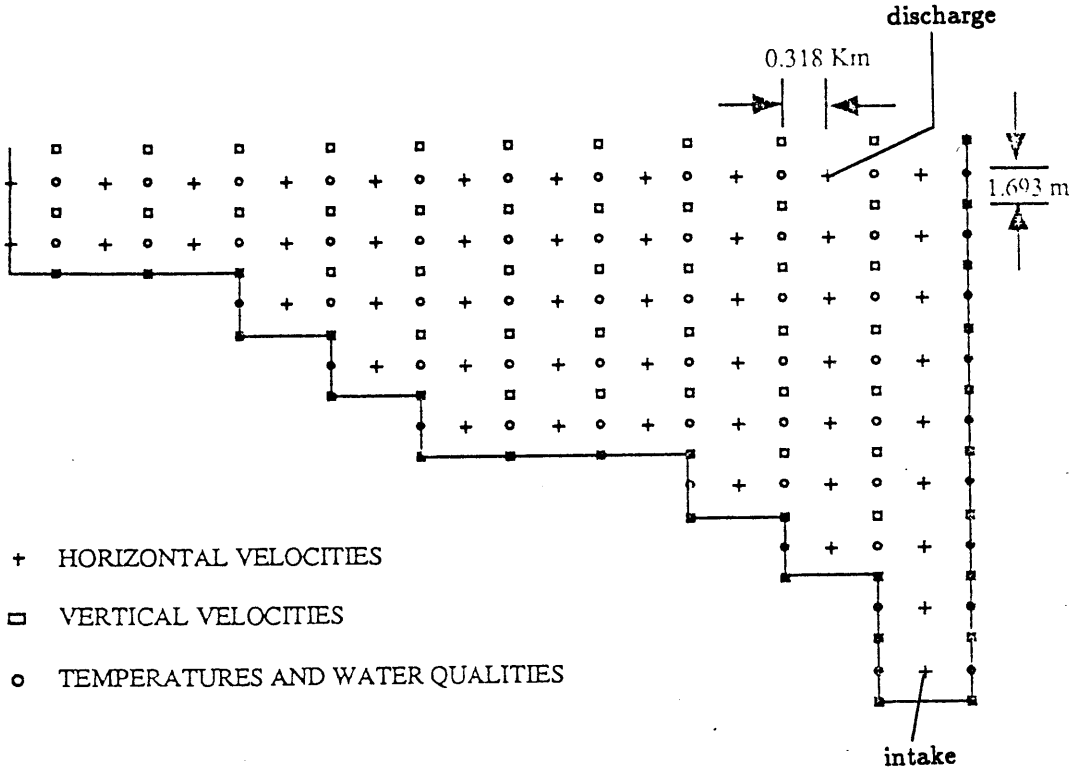

Figure 5-1 Schematization of Mount Storm Lake for 2-D model

0.67 km. The vertical interval between each of the nine horizontal layers is about 3.4 m. In this two-dimensional model, it was also necessary to supply data on the breadth of the lake at each station for all eleven crossections. Since the grid is staggered, there are two adjacent horizontal velocity points and two adjacent vertical velocity points for each temperature or water quality grid point. The horizontal and vertical computational intervals adopted for the model are $\Delta x =$ 0.318 km and $\Delta z = 1.524$ m, respectively. The time step is restricted by the CFL condition,

$$\Delta t \leq \frac{\Delta x}{(gH_{max})^{\frac{1}{2}}} \tag{5.20}$$

For the averaged lake depth of 12 m, $\Delta t \lesssim 30$ s.

5.2.2 Modifications to the Model

There were a few modifications made to the two-dimensional model for application Mount Storm Lake. In order to ensure that the comparison with MITEMP was appropriate, the terms describing the individual heat flux components in NARES were changed to correspond with those in MITEMP. Also the values of two parameters, the von Karman constant and β, the portion of the solar radiation absorbed near the surface, were changed from 0.35 and 0.55 to 0.4 and 0.5, respectively. The model was also modified to compute the temperature of the discharge from the station generation data as was described for MITEMP in Chapter 2. Model viscosities and dispersion coefficients were chosen based on the calibration at the Wanaque Reservoir (Huang et al., 1988): $N_x = K_x = 10^5 cm^2/s$, $N_z = K_z = 0.01$ cm^2/s. There was insufficient time to do a full calibration and

verification of this model. Therefore the temperature structure rather than the accuracy of the two models was compared.

5.3 Results

The model was run with one year's data (Sept. 1987 - Aug. 1988). A typical longitudinal-vertical temperature section is shown in Figure 5.2 (t = 45 d) in comparison with initial conditions shown in Figure 5.3. The effect of cooling is apparent as the range of temperatures is now about 20-25° C compared with the initial conditions of about 29-35° C. The vertical temperature profiles at the same time—that is, after 45 days—are shown in Figure 5.4.

The maximum longitudinal temperature difference in the observed data below the epilimnion is about 2° C (see Figures 3.2-3.8 as well as Figure 5.3). The model predicts a similar range in temperature difference in the hypolimnion. Therefore, the 2-D model simulates an improved thermal structure in the hypolimnion. Also the model is better able to represent the actual position of the discharge. This is in contrast to the 1-D model MITEMP which assumes that the discharge is at the head of the lake.

In conclusion, though, there appears to be little advantage to using the more complex model for this lake and the existing power plant configuration. On the other hand, the 2-D model would be the better model to use if we were contemplating a substantial change in either discharge or intake positions. For example, it would provide information about where the temperatures are lowest (for an intake). However, the model would require substantial calibration and validation.

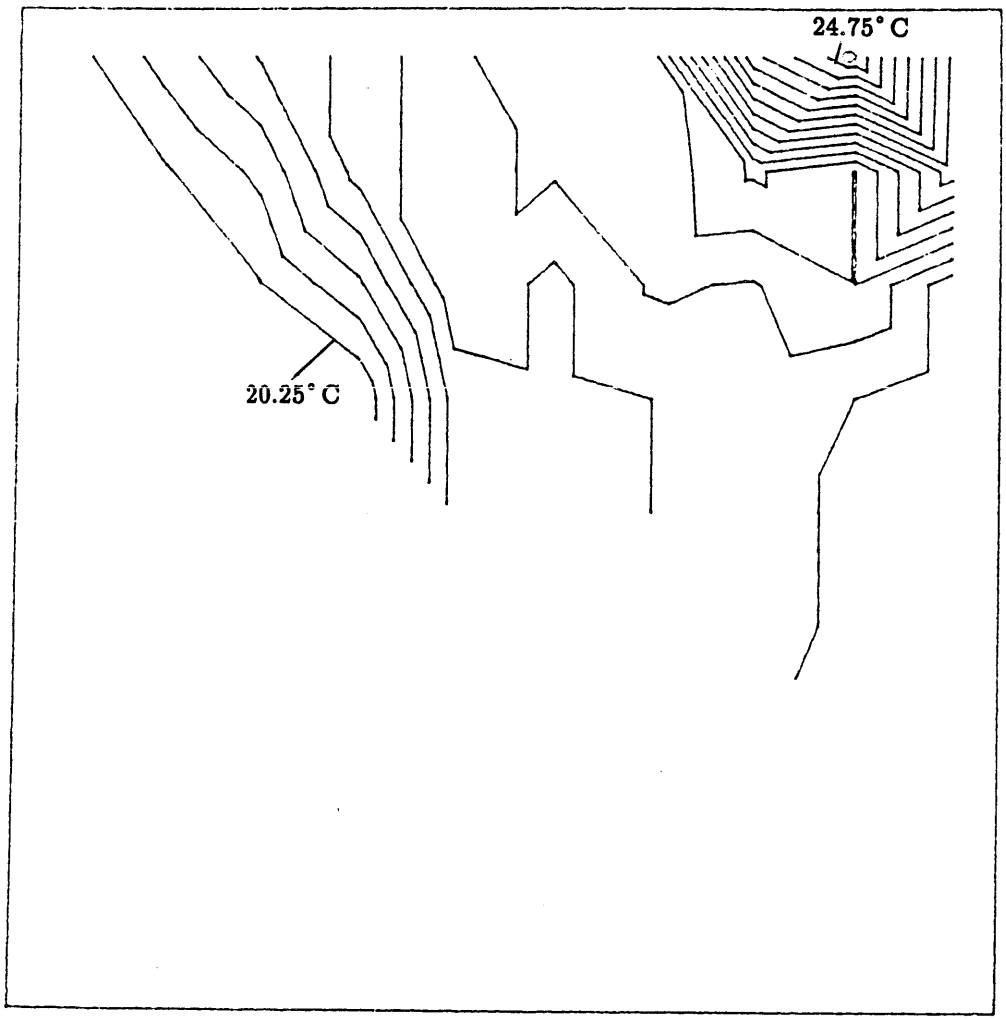

Figure **5-2** Temperature contours after 45 days (Δtemp = 0.25° C)

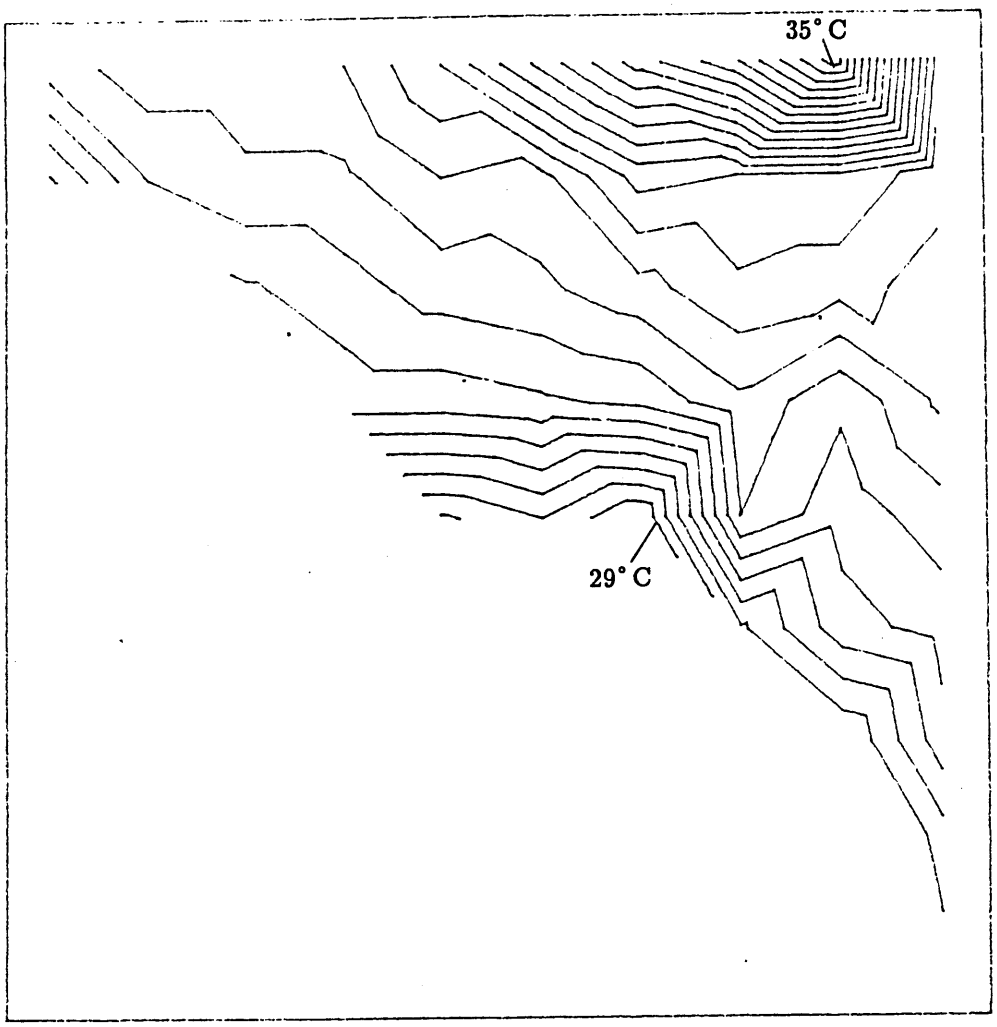

Figure **5-3** Initial temperature in Mt. Storm Lake (Sept. 1, 1986)

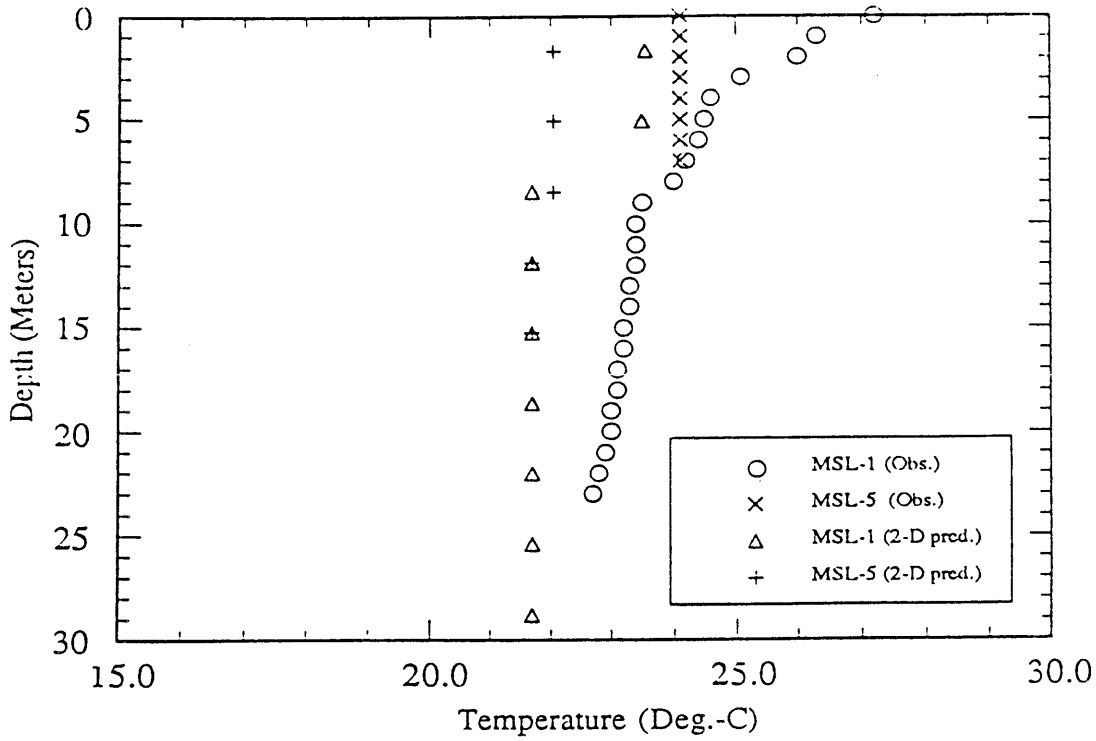

Figure 5-4 Comparison of 2-D model temperature profiles after 45 days

6 SUMMARY AND CONCLUSION

The Mount Storm Station is a three-unit electric generating station that is owned by Virginia Power. The company is considering several options for increasing power generation at the station and a reliable thermal model of Mount Storm Lake is required to assess compliance with discharge temperature limits. Such a model would also be useful to assess the resulting biological impacts on the lake. The physical characteristics of the lake suggest a one-dimensional structure below a heated surface layer. Therefore the emphasis of this study was on the modification and calibration of a basically 1-D model (MITEMP) for this purpose.

Using the method of pond classification described by Jirka et al. (1978), Mount Storm Lake is schematized in MITEMP as a deep vertically stratified cooling pond. Details concerning this model are described in Chapter 2. The initial model predictions for the first simulation year (Sept. 1986 - Aug. 1987) were shown in Chapter 3 to be quite good with the mean error at three locations being about -0.6° C and the standard deviation being about 1.1° C. The small differences between observation and model predictions were assumed to be due to a combination of insufficient seasonal distribution of heat input to the model and insufficient mixing. Subsequent model calibration aiming at improving the performance of the model confirmed this. Comparison of calculated solar radiation with solar radiation measurements showed that the former had a seasonal bias and an average error of 17%. Correction for the solar radiation reduced the mean error from -0.6° C to 0.03° C. Model sensitivity was also showed that the goodness of fit of the model output could be improved by reducing the Fischer estimate of longitudinal dispersion in the upper layer by a factor of 4, and increasing the entrance-dilution coefficient from 2 to 2.15. The mean of the average errors after the calibration was increased to about -0.2° C with a standard deviation of

about 1.2° C. However, the range of the errors across the epilimnion was reduced from 0.94° C to 0.47° C.

The time series of the errors were evaluated at three representative locations: near the discharge, at the end of the surface layer region, and at the mean lake bottom. A Fourier analysis of these errors showed little periodicity at an annual cycle, but the errors were found to be significantly correlated with the "observed" station generation. As a result, a linear regression was computed that may be applied to the model. Using this regression, the variance of the recalibrated model is reduced by about 25% at MSL-1 (surface) for the first year.

The model verification using the second year of data also indicates good accuracy. The mean of the average errors using the calibrated model is 0.11° C with a standard deviation and a root-mean-square error of about 1.5° C. The latter is an estimate of the model accuracy if the model were applied to additional years' data without any further calibration. The mean error was reduced to -0.06° C using the linear regression. It is suspected that either the station generation data are slightly inaccurate or, more likely, that an error is introduced by the assumed linearity between power production and heat rejection, in the model input.

Several scenarios being considered by Virginia Power involve current and future electricity production that would increase water consumption at Mt. Storm Lake, which would in turn result in increased water temperatures due to reduced lake surface area. A 0-D steady-state model based on monthly averages of meteorological data was developed at an earlier stage of this project to examine this effect. In Chapter 4 the damping resulting from the use of averaged data in the steady state was compared to the thermal inertia provided by the transient model. The result shows that an averaging interval of 30 days provided relatively good estimates of the water

temperature with an RMS accuracy of about 2.5° C. Considering the extremely fast run times, one concludes that the 0-D model was a useful and efficient screening model.

In Chapter 5, the 1-D model was also compared with a 2-D model to see what changes in thermal structure result from an improved description of the flow field. There was insufficient time to fully evaluate the 2-D model but initial comparison suggested an improvement in the description of the spatial structure. However, since the maximum observed horizontal temperature variation is only about 2.0° C, the detailed description of the flow field is not of primary importance in modeling the temperature in Mount Storm Lake.

For the outlined purposes of this study, the 1-D model (MITEMP) is probably as accurate and definitely more efficient in describing the lake response than would be the 2-D model. The run time for MITEMP to simulate a whole year with daily time steps is about 3 CPU minute on the microVax. On the other hand, the 2-D model requires a time step of less than 30 seconds for stability reasons and requires over 14 hours of CPU time for a simulation length of one year. It is apparent that in comparison with the 1-D model this model does not make an efficient use of computer time. As stated by Wang and Kravitz (1980), "the long-term (> 1 month) simulation can be very costly" using the 2-D model.

This does not imply that 2-D models are not useful. The major difference resulting from the assumptions inherent in the three models is that in the 0-D and 1-D model, there is no need for any momentum equations; in the 0-D model the reservoir is assumed to be well-mixed and in the 1-D model the flow field is presumed. The 2-D model is therefore useful for the description of water bodies in which the flow field is more complex than can be adequately described by simple schematization (for example, estuarine circulation for which the original model was developed) or when the spatial

distribution in the hypolimnion is important for purposes of locating plant discharge and intake. Although the flow field of Mount Storm Lake may be better described, in principle, by the 2-D model, the 1-D model appears to be sufficiently accurate for the purposes for which a model was required and it does not appear that much greater accuracy may be achieved by the more complex model. Indeed, the 2-D model results themselves suggest that the thermal structure prescribed by the 1-D model is appropriate.

7 REFERENCES

Adams, E. E., O. M. Adelaja. 1989. Future water availability at Mount Storm Lake. Report for Virginia Power Co.

Adams, E. E., D. R. F. Harleman, G. H. Jirka, K. D. Stolzenbach. 1981. Heat disposal in the water environment. Lecture Notes, R. M. Parsons Laboratory, MIT, Cambridge, Mass.

Adams, E. E., A. D. Koussis. 1980. Transient analysis for shallow cooling ponds. *J. Energy Div., ASCE* 106(EY2):141-153.

Adams, et al. 1987. Analysis of evaporation data from heated ponds. Electric Power Research, Report No. EPRI CS-5171.

Christodoulou, G. C., J. J. Connor, B. R. Pearce. 1976. Mathematical modeling of dispersion in stratified waters. MIT SG 76-14.

Edinger, J. R., J. G. Geyer. 1965. Cooling water studies for Edison Electric Institute. Johns Hopkins University, Project No. RP-49, Heat Exchange in the Environment.

Fischer, H. B. 1967. The mechanics of dispersion in natural streams. *J. Hydr. Div., ASCE* 93(HY6).

Gilbert/Commonwealth Assoc. 1985. Virginia Power Mt. Storm station lake temperature study, IR-6841.

Hamon, R. W., L. L. Weiss, W. T. Wilson. 1954. Insolation as an empirical function of daily sunshine duration. *U.S. Weather Bureau Monthly Weather Review* 82(6).

Harvey, R. L., R. W. Davies. 1976. The role of surface mixing in the seasonal variation of the ocean thermal structure. *J. Phys. Oceanogr.* 6:504-510.

Helfrich, K. R., E. E. Adams, A. L. Godbey, D. R. F. Harleman. 1982. Evaluation of models for predicting evaporative water loss is cooling impoundments. Electric Power Research Institute Report No. EPRI CS-2325.

Ho, E. K., E. E. Adams. 1984. Final calibration of the cooling lake model for North Anna Power Station, R. M. Parsons Laboratory, MIT, Technical Report No. 295.

Huang, P. S., T. O. Najarian, V. K. Gunawardana. 1988. Influence of Wanaque south diversion on the trophic level of Wanaque Reservoir and its water quality management program. Report prepared for North Jersey District Water Supply Commission and Hackensack Water Company.

Jirka, et al. 1977. Analysis of cooling effectiveness and transient long-term simulations of a cooling lake. R. M. Parsons Laboratory, MIT, Technical Report No. 232.

Jirka, G. H., et al. 1978. Mathematical predictive model for cooling ponds and lakes, Part A: Model development and design considerations. R. M. Parsons Laboratory, MIT, Technical Report No. 238.

Jirka, G. H., E. E. Adams, K. D. Stolzenbach. 1981. Buoyant surface jets. *J. Hydr. Div., ASCE* 107(HY11):1467-1487.

Kasten, F. 1964. A new table and approximation formula for the relative optical air mass. U.S. Army Material Command, Cold Regions Research and Engineering Laboratory, Technical Report No. 136.

Luxenberg, R. R., E. E. Adams. 1986. Hydrothermal performance of vertically stratified cooling ponds. Electric Power Research Institute Report No. EPRI CS-4320.

Octavio, K. A. H., G. H. Jirka, D. R. F. Harleman. 1977. Vertical heat transport mechanisms in lakes and reservoirs. R. M. Parsons Laboratory, MIT, Technical Report No. 227.

Octavio, K. H., et al. 1980. Mathematical predictive models for cooling ponds and lakes, Part B: User's manual and application of MITEMP. R. M. Parsons Laboratory, MIT, Technical Report No. 262.

Ryan, P. J., D. R. F. Harleman. 1973. An analytical and experimental study of transient cooling pond behavior. R. M. Parsons Laboratory, MIT, Technical Report No. 161.

Ryan, P. J., D. R. F. Harleman, K. D. Stolzenbach. 1974. Surface heat loss from cooling ponds. *Water Res. Res.* 10(5).

Swinbank, W. C. Long-wave radiation from clear skies. 1963. *J. Royal Met. Soc.* 89.

Thérien, N. 1981. Simulating the environmental impact of a large hydroelectric project. *Simulation Proceedings Series* 9(2).

Wang, D. P., D. W. Kravitz. 1980. A semi-implicit two-dimensional model of estuarine circulation. *J. Phys. Oceanogr.* 10:441-454.

Watanabe, M., D. R. F. Harleman, J. J. Connor. 1975. Finite element model for transient two-layer cooling pond behavior. R. M. Parsons Laboratory, MIT, Technical Report No. 203.

Wells, S. A., E. E. Adams, D. R. F. Harleman. 1982. Calibration and verification of the cooling lake model for North Anna Power Station. R. M. Parsons Laboratory, MIT, Technical Report No. 272.

Wunderlich, W. O. 1972. Heat and mass transfer between a water surface and the atmosphere. TVA Engineering Laboratory Laboratory Report No. 14.

Zaric, Z. P. 1978. *Thermal disposal from power generations.*

APPENDIX. CLASSIFICATION OF MOUNT STORM LAKE

A method of pond classification as described by Jirka et al. (1978) is illustrated in Figure A-1. Dependent on their thermal structure, cooling ponds may be classified as deep (fully stratified), intermediate (partial), and shallow (vertically fully mixed). It is important to note that classification is dependent not only on actual depth but also on pond shape, size, loading rate, and discharge structure.

A.1 Artificial Heat Loading Criterion, ϕ

A concentrated artificial heat source, such as a plant discharge, will produce horizontal temperature variation in an impoundment. The strength of the horizontal variability depends on the relative magnitude of the heat source when compared to the surface area. The parameter ϕ is defined as

$$\phi = \text{artificial heat source/Pond surface area (MWt/acre)}$$

ϕ allows one to distinguish between ponds whose hydrothermal structure is influenced primarily by natural forces such as surface wind stress as opposed to power plant circulation. For Mount Storm,

$$\phi \sim 1.87\text{MWt/acre}$$

A.2 Pond Number, $\mathbb{P}$

The pond number is defined as

$$\mathbb{P} = \left[\frac{f_i Q_0^2}{4\beta\Delta T_0 g H^3 W^2} D_v^3 \frac{L}{H}\right]^{\frac{1}{4}}$$

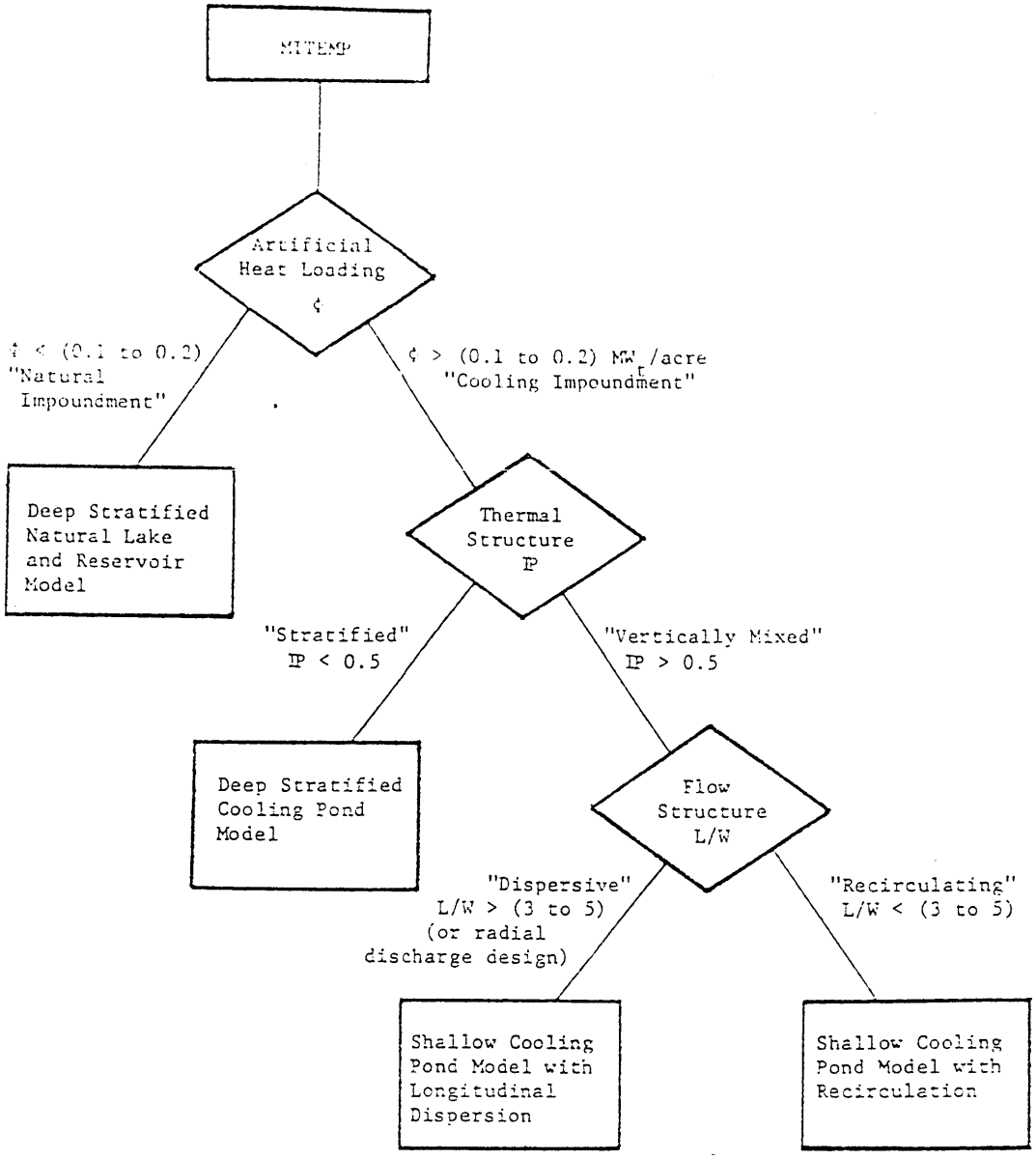

Figure A-1 Hierarchical structure of MITEMP and decision criteria

where the parameters are f_i, interfacial friction factor = 0.01 for field applications; Q_0, condenser flow rate = 49 m^3/s; D_v, volumetric dilution caused by entrance mixing = $1.2F_0$ - 0.2 (Jirka et al., 1981); β, coefficient of thermal expansion = $2 \times 10^{-4}/°C$; ΔT_0, condenser temperature rise = 10.16° C; g, the acceleration of gravity = 9.81 m/s^2; H, the characteristic pond depth = 13.4 m; W, characteristic pond width ~ 700 m; L, characteristic pond length = ~7000 m; and F_0 is a discharge densimetric Froude number defined as

$$F_0 = \frac{u_0}{\sqrt{\beta \Delta T_0 g (h_0 b_0)^{\frac{1}{2}}}}$$

where h_0 = discharge depth; b_0 = jet half width for symmetric discharge.

$\mathbb{P}$ represents the ratio of the surface layer thickness, h_s, to the average pond depth, where h_s is derived as the heated water depth necessary to calculate the condenser flow across the pond by buoyant gravitational convection.

For Mount Storm Lake

$$u_0 = Q_0/A_0$$

where A_0 is the crossectional area of the discharge jets,

$$A_0 = 2\left[\frac{\pi}{4}(D_1^2 + 2D_2^2)\right]$$

D_1 - Diameter of 2 Unit 3 pipes, 3.05 m

D_2 - Diameter of 2 Unit 1 and Unit 2 pipes, 2.74 m

and

$$F_0 = 4$$

$$D_v = 4.6$$

$$\mathbb{P} = \left[0.89\frac{L}{W^2}\right]^{\frac{1}{4}}$$

For the lake schematized above, L = 10W and $\mathbb{P} = 0.33$. If it was assumed that L = W, then $\mathbb{P} = 0.19$. Therefore $0.19 \leq P \leq 0.33$ and Mount Storm Lake may be described as a vertically stratified lake.